Energy Reports 7 (2021) 3979–3997

Contents lists available at ScienceDirect

Energy Reports

journal homepage: www.elsevier.com/locate/egyr

Research paper

Gradient-based optimization with ranking mechanisms for parameter identification of photovoltaic systems

Iman Ahmadianfar [a], Wenyin Gong [b], Ali Asghar Heidari [c,1], Noorbakhsh Amiri Golilarz [d], Arvin Samadi-Koucheksaraee [a], Huiling Chen [e,*]

[a] Department of Civil Engineering, Behbahan Khatam Alanbia University of Technology, Behbahan, Iran
[b] School of Computer Science, China University of Geosciences, Wuhan 430074, China
[c] School of Surveying and Geospatial Engineering, College of Engineering, University of Tehran, Tehran 1439957131, Iran
[d] School of Computer Science and Engineering, University of Electronic Science and Technology of China, Chengdu 611731, China
[e] College of Computer Science and Artificial Intelligence, Wenzhou University, Wenzhou, Zhejiang 325035, China

ARTICLE INFO

Article history:
Received 27 February 2021
Received in revised form 1 June 2021
Accepted 14 June 2021
Available online xxxx

Keywords:
Photovoltaic models
Parameter identification
Gradient-based optimizer
Optimization
Swarm intelligence

ABSTRACT

Deriving optimal photovoltaic (PV) models' optimal parameters have tremendous significance in simulating, evaluating, and controlling the photovoltaic systems. Determining unknown parameters of these PV models is a multimodal, nonlinear, and complex optimization problem. Hence, developing a robust optimization model to achieve optimal parameters of the PV models effectively is essential. This paper proposes an enhanced metaphor-free gradient-based optimizer (EGBO) for extracting PV parameters quickly, precisely, and reliably. In the EGBO, a rank-based mechanism is employed to update its parameters efficiently. Also, the logistic map (LC) is implemented to better use the local escaping operator (LEO) in the original GBO algorithm. The proposed EGBO optimally identifies various parameters in the PV model, such as single diodes, double diodes, and PV modules. The relevant results indicate that compared with most advanced optimization methods, the EGBO algorithm is competitive in reliability, accuracy, and convergence speed. Moreover, the relevant results from the experimental data drawn from the manufacturer's datasheet demonstrate that the developed approach can offer highly accurate solutions at various irradiances and temperatures. Consequently, the achieved results confirm that the novel approach can be presented as a utility tool for deriving optimal PV models' optimal parameters, and it can be helpful in modeling PV systems.

1. Introduction

Considering some critical challenges, such as but not limited to environmental pollution, energy crisis, fuel exhaustion, climate change, we will understand the significance of renewable energy sources in which they play an essential role in our daily life. As a clean and attainable renewable energy source, PV is categorized among the most potential cell-based energy sources (Xu and Wang, 2017; Hu et al., 2019). Progression in photovoltaic technology provides us with nonlinear solar cells' nonlinear characteristics based on estimating the parameters and modeling precisely, which attracted lots of attention in various approaches such as control and photovoltaic systems' maximum power point tracking (Campana et al., 2019; Gao et al., 2018). Selecting a PV system is very important in the PV model (Muhsen et al., 2016; Qais et al., 2019a) due to imitating the actual photovoltaic cells' manner and behavior (Chin et al., 2015). The single diode model (SDM) and the double diode model (DDM) are categorized among the most commonly adopted PV models (Humada et al., 2016). Admittedly, extracting the parameters rapidly, reliable, and precise is very significant in these models. A plus point is that the existing PV models' formula is nonlinear and implicit (Jiang and Chen, 2016), which is challenging. Thus, designing a promising and effective model for recognizing and identifying these parameters is required.

When there are several valid solutions for the same problem, we need to provide several searching trends to scan the search space deeply. Such problems are open in many domains such as image segmentation (Rodriguez-Esparza et al., 2020; Zhao et al., 2020a,b), risk prediction (Zhang et al., 2020a), nonlinear systems (Zhang et al., 2020b), thermal recovery technology (Deng et al., 2021), variational analysis (Huang et al., 2021), and sliding-mode control (Qu et al., 2021). Optimization field philosophy is

* Corresponding author.
E-mail addresses: i.ahmadianfar@bkatu.ac.ir (I. Ahmadianfar), wygong@cug.edu.cn (W. Gong), as_heidari@ut.ac.ir (A.A. Heidari), noorbakhsh.amiri@std.uestc.edu.cn (N.A. Golilarz), arvinsamadi.k@gmail.com (A. Samadi-Koucheksaraee), chenhuiling.jlu@gmail.com (H. Chen).
[1] https://aliasgharheidari.com.

https://doi.org/10.1016/j.egyr.2021.06.064

based on progressive improvement in the current state of the event until a better solution be reached (Xue et al., 2020). Hence, it is possible to convert the parameter extraction problem for PV cell and module models into an optimized-based model with a defined objective function. The presence of noise in the estimated current voltage resulting in nonlinear search space and multiple local optimal (Niu et al., 2014), so that modeling one parameter estimation technique will be challenging (Yu et al., 2017a). In a general view, to measure photovoltaic models' parameters, deterministic methods and metaheuristic methods can be exploited. In the deterministic approach, Newton (Easwarakhanthan et al., 1986), Levenberg Marquardt (Dkhichi et al., 2014), and the conjugate direction method (Hestenes and Stiefel, 1952) are the most well-known techniques that many gradient computations are required in these approaches. These methods act promisingly while tackling the local search. In opposite, reaching to local optimum will be done quickly. Due to this issue, the solutions' preciseness will be avoided in the algorithm in the iterations, consequently (Ahmadianfar et al., 2019a; Abbassi et al., 2019; Chen and Yu, 2019; Ahmadianfar et al., 2019b). The initial point plays a crucial role in these techniques. Therefore, both the solutions' accuracy and the convergence rate are affected by the initial points' choice (Song et al., 2020). A convex characteristics-based fitness function is also required to utilize and employ the cited techniques, which reduces the broadness of their applications. Meta-heuristic approaches have been utilized to address these drawbacks and limitations, and they performed well compared with some conventional techniques (Ahmadianfar et al., 2020a; Heidari et al., 2019a; Zhao et al., 2019a). Swarm based approaches are very wide nowadays (Aljarah et al., 2020; Mafarja et al., 2020; Shan et al., 2021; Tu et al., 2021), but some of the best methods in design are not limited to Harris hawk optimization (HHO)[2] (Heidari et al., 2019a; Chen et al., 2020a), slime mould algorithm (SMA)[3] (Li et al., 2020a; Zhang et al., 2021a; Zhao et al., 2021; Yu et al., 2021a), hunger games search (HGS)[4] (Yang et al., 2021), and Runge Kutta optimization (RUN)[5] (Ahmadianfar et al., 2021). Researchers used to employ these solvers in the system for evaluating and determining the parameters in many areas such as FACTS optimization (Jordehi and Jasni, 2012), feature selection (Hu et al., 2021; Li et al., 2017; Zhang et al., 2020c,d), the hard maximum satisfiability problem (Zeng et al., 2011, 2012), wind speed prediction (Chen et al., 2019a), engineering design problems (Ba et al., 2020; Gupta et al., 2019; Liang et al., 2020; Nautiyal et al., 2021; Zhang et al., 2020e), medical data classification (Hu et al., 2017; Li et al., 2018; Zhao et al., 2019b), bankruptcy prediction (Wang et al., 2017a; Xu et al., 2019; Yu et al., 2021b; Zhang et al., 2020j), PID optimization control (Zeng et al., 2014, 2015, 2019), gate resource allocation (Deng et al., 2020a), parameter optimization (Heidari et al., 2019b; Wang et al., 2017b), image segmentation (Zhao et al., 2020a,c), fault diagnosis of rolling bearings (Deng et al., 2020b; Zhao et al., 2019c), prediction problems in educational field (Wei et al., 2020; Zhu et al., 2020; Lin et al., 2019; Tu et al., 2019; Wei et al., 2017), and scheduling problem (Pang et al., 2018; Zhou et al., 2018).

An improved adaptive differential evolution (IADE) optimizer combined with fitness value's feedback-based structure has been proposed in Jiang et al. (2013) to identify solar modules' parameters. Additionally, for measuring and estimating the solar modules' parameters, a chaotic particle swarm optimization (CPSO) (Wei et al., 2011) has been introduced to improve local convergence capability and the global search. Simulated annealing (SA) is used first to recognize the solar cell parameters, then to see the performance analysis of the SA model, SDM, DDM, and PVM are used consequently (El-Naggar et al., 2012). A bacterial foraging algorithm (BFA) has been developed by Rajasekar et al. (2013) to imitate the characteristics and features of the photovoltaic solar cell. They showed that the BFA has a better performance for the derivation of model parameters than the genetic algorithm (GA) and artificial immune system (AIS). Oliva et al. (2014) developed an artificial bee colony (ABC) to identify parameters of the solar cells. The results showed that the ABC algorithm has a better efficiency compared with the harmony search, particle swarm optimization (PSO), GA, and BFA. For extracting, the photovoltaic modules' parameters accurately and precisely, a backtracking search algorithm (BSA) based on multiple-learning has been introduced in Yu et al. (2018). They demonstrated that the proposed MLBSA could provide more accurate results compared with three variants of BSA, namely improved BSA (IBSA) (Nama et al., 2017), learning BSA (LBSA), and oppositional BSA (OBSA). A novel hybrid teaching-learning-based artificial bee colony (TLABC) introduced by Chen et al. (2018) was used to estimate the photovoltaic parameters. Experimental results indicated that the proposed algorithm has a very competitive efficiency in terms of reliability and precision. Li et al. (2019a) developed an improved teaching learning-based optimization (ITLBO) for extracting the optimal parameters in photovoltaic models. They compared the results obtained by the ITLBO with improved JAYA (Yu et al., 2017b), MLBSA, TLABC, self-adaptive TLBO (SATLBO) (Yu et al., 2017a), TLBO with learning experience (LETLBO) (Zou et al., 2015), and generalized oppositional TLBO (GOTLBO) (Chen et al., 2016). The results indicated the suitable performance of the ITLBO to extract the parameters of PV models. Also, a random learning gradient based optimization designed recently that shows efficient results for design of photovoltaic models (Zhou et al., 2021). Zhang et al. introduced a novel moth flame optimization (MFO) algorithm based on orthogonal strategy and Nelder–Mead simplex (NMS) to estimate parameters of photovoltaic modules (Kordestani and Zhang, 2020). The performance analysis indicated the metaheuristic approaches' superiority over other alternative methods in extracting photovoltaic models' parameters. Several recent optimizers based on HHO and MFO also revealed a top performance for PV problems (Abbassi et al., 2019; Jiao et al., 2020; Abbassi et al., 2020; Chen et al., 2020b; Ridha et al., 2020; Zhang et al., 2020f).

Li et al. (2020) introduced a hybrid adaptive teaching-learning-based optimization and differential evolution (ATLDE) to identify the parameters of PV models. They demonstrated the high efficiency of the proposed optimizer compared with the DE, jDE, JADE, TLBO, GOTLBO, and SATLBO. Selem et al. (2021) used the artificial electric field algorithm (AEFA) to determine nine parameters of triple-diode (TDM) PV model. Their results illustrated that the proposed AEFA can be considered a suitable tool for optimizing the TDM parameters. Qais et al. (2020a) combined the computation and Harris hawks optimization (HHO) algorithm to derive the parameters of PV models. The results indicated that the proposed algorithm could be effectively used to specify the parameters of PV panels. Qais et al. (2020b) employ the transient search optimization (TSO) to estimate PV modules' parameters. They showed that the TSO algorithm was a useful method to find the optimal parameters of TDM. Sunflower optimization (SFO) algorithm has been used by Qais et al. (2019b) to identify electrical parameters of TDM. Their simulation results demonstrated a suitable agreement with the measured dataset.

The above algorithms' parameters can affect their performance, but they still perform promisingly and give favorable results. Setting a suitable and proper parameter for a new and specific optimizer is a critical task, which is very difficult—

[2] https://aliasgharheidari.com/HHO.html
[3] https://aliasgharheidari.com/SMA.html
[4] https://aliasgharheidari.com/HGS.html
[5] https://aliasgharheidari.com/RUN.html

additionally, tuning and controlling the parameters in an inappropriate way results in obtaining the local optimum and increasing computational cost and effort (Yang et al., 2021). Decision space's topography may easily lead the algorithm to a deceitful optimum (Ma et al., 2021). Thus, the quality of the solutions cannot be improved by even more iteration. Eventually, another challenging task causing the problem to be tackled not in an easy way is identifying the parameters of the photovoltaic model, and it is a kind of multimodal problem that includes various local optimum—after that, reaching a global optimum solution is troublesome for a broad range of meta-heuristic optimization algorithms. Researchers are looking for a promising algorithm to identify various photovoltaic models' parameters with a favorable computational time to address all these issues.

A gradient-based optimizer (GBO) has been proposed by Ahmadianfar et al. (2020a), which has been regarded as a metaphor-free and efficient optimization algorithm. This algorithm's central concept is based on the gradient-based Newton's technique that local escaping operator (LEO) and gradient search rule (GSR) are its two principal operators. The GSR is implemented to search in the solution space globally, and the LEO is used to avoid local solutions. The main advantage of this algorithm is in implementing two novel operators to move toward promising regions in the solution space. The GBO uses an adaptive mechanism to set the control parameters are each iteration; this machine is suitable for many problems (Ahmadianfar et al., 2020a), but according to the No Free Lunch (NFL) theorem, it may not solve some other problems very well. Thus, we introduce an enhanced version of GBO (EGBO) to address and solve the problems of parameter extraction of the photovoltaic model accurately and quickly, which gives promising and satisfactory results. In the proposed EGBO algorithm, we have utilized a rank-based mechanism for assigning F values to each individual more rationally. Next, we applied a chaotic map for randomly utilizing the LEO mechanism. The proposed EGBO algorithm is an efficient method while to extract some parameters of various photovoltaic models. The results demonstrate the superiority of this algorithm over other alternative meta-heuristic algorithms.

The main contributions are as below:

– At first, we introduced an improved and extended version of gradient-based optimization (EGBO) for extracting the PV parameters, and this algorithm consists of a rank-based mechanism for assigning ρ values to each population's individual more efficiently.

- We have applied a chaotic map to the algorithm to improve the solution's quality, speed of the convergence rate, and searching capability of the exploitation phase.
- The EGBO algorithm's performance analysis has been appropriately examined by extracting various photovoltaic models' parameters with two photovoltaic models at various temperatures and irradiance.
- Consequently, to address and solve the identification issue of the photovoltaic model's parameters, an effective and promising approach has been presented.

This research is structured as follows. Firstly, Section 2 is about the description of SDM, DDM, and some objective functions. In Section 3, we addressed the original GBO algorithm. Then, the proposed improved GBO algorithm is fully described in Section 4. Eventually, Section 5 delivers the experimental analysis, results, and discussions, and Section 6 is the whole paper conclusion.

2. Problem statement

Based on Section 1, there are two main common and popular modes: SDM and DDM. This section also includes describing the SDM, DDM, and SDM based on photovoltaic module (SMM) and the objective function.

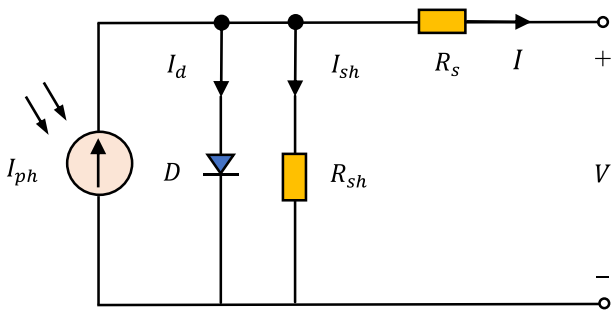

Fig. 1. Equivalent circuit diagram of the SDM model.

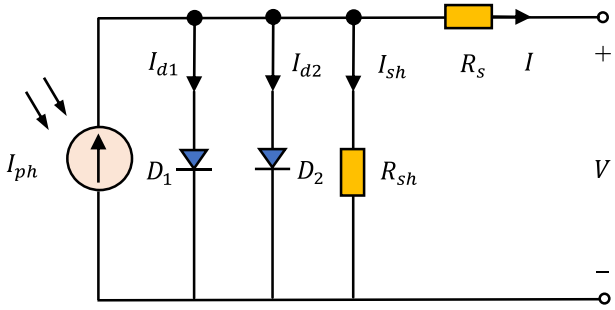

Fig. 2. Equivalent circuit diagram of DDM model.

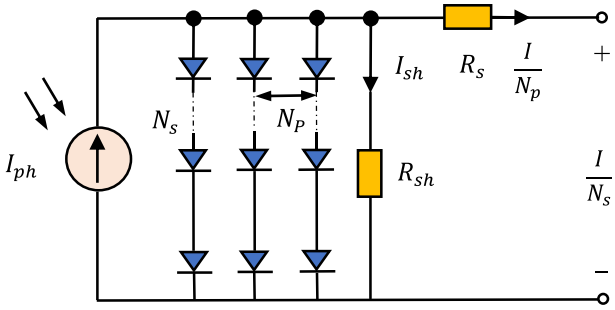

Fig. 3. Equivalent circuit diagram of the SMM model.

2.1. Single diode model

SDM is a widely used model for extracting, explaining, and expounding the solar cells' features due to its structure, which is simple, and its high accuracy and precision (Fan et al., 2021; Liu et al., 2020, 2021; Ridha et al., 2021b). Fig. 1 shows the SDM's equivalent circuit. As can be seen from the diagram, the architecture of SDM is for reflecting the losses corresponding to the load current, which is based on incorporating the current source with the diode, a shunt resistor for displaying the leakage current, and an electric resistance battery. SDM's output current is given by Eq. (1) (Yu et al., 2017a):

$$I = I_{ph} - I_d - I_{sh} \tag{1}$$

where I refers to the output current, I_{ph} is the photo-produced current, I_d is the diode current, and I_{sh} is the shunt resistor current, described as below,

$$I_d = I_o \left[\exp\left(\frac{V + IR_s}{\alpha V_t} \right) - 1 \right] \tag{2}$$

$$I_{sh} = \frac{V + IR_s}{R_{sh}} \tag{3}$$

Table 1
Objective function and variables of different PV models.

PV model	Objective function	Variables
	$f(V, I, x)$	x
SDM	$I_{ph} - I_o\left[\exp\left(\frac{V+IR_s}{\alpha V_t}\right) - 1\right] - \frac{V+IR_s}{R_{sh}} - I$	$(I_{ph}, I_o, R_s, R_{sh}, \alpha)$
DDM	$I_{ph} - I_{o1}\left[\exp\left(\frac{V+IR_s}{\alpha_1 V_t}\right) - 1\right] - I_{o2}\left[\exp\left(\frac{V+IR_s}{\alpha_2 V_t}\right) - 1\right] - \frac{V+IR_s}{R_{sh}} - I$	$(I_{ph}, I_{o1}, I_{o2}, R_s, R_{sh}, \alpha_1, \alpha_2)$
SMM	$I_{ph} - I_o\left[\exp\left(\frac{V+IR_sN_s}{\alpha N_s V_t}\right) - 1\right] - \frac{V+IR_sN_s}{R_{sh}N_s} - I$	$(I_{ph}, I_o, R_s, R_{sh}, \alpha)$

where I_o denotes the reverse saturation current of the diode, α is the diode ideality factor, R_s refers to series resistance, R_{sh} denotes to shunt resistance, V is the output voltage of the cell, and V_t is the junction thermal voltage given below,

$$V_t = \frac{k \times T}{q} \tag{4}$$

where T is the junction temperature in Kelvin, k refers to the Boltzmann constant ($1.3806503 \times 10^{-23}$ J/K), and q is the electron charge ($1.60217646 \times 10^{-19}$ C).

The output current I is formulated in Eq. (5) based on the combination of the above-described equations, whereas it is obvious there are several unknown parameters as (I_o, I_{ph} R_s, R_{sh}, and α), which are required to be derived and extracted in SDM.

$$I = I_{ph} - I_o\left[\exp\left(\frac{V + IR_s}{\alpha V_t}\right) - 1\right] - \frac{V + IR_s}{R_{sh}} \tag{5}$$

2.2. Double diode model (DDM)

The recombination current loss effect in the blocking layer is not considered in the SDM. Thus, to address this issue and consider this loss, DDM as an accurate model is introduced by Chen et al. (2016). In this method, the two primary diodes operate with the PV and shunt currents in parallel. The operation of these diodes is described as follows, where one works as a rectifier and the other is designed to mimic the recombination of current charges and some uncontrollable factors. Fig. 2 notes the DDM's equivalent circuit. Like the previous studies, the output current is formulated by Eq. (6) (Jiang and Chen, 2016):

$$I = I_{ph} - I_{d1} - I_{d2} - I_{sh} \tag{6}$$

where I_{d1} refers to the first diode current, and I_{d2} is the second diode currents, which are described in detail as below,

$$I_{d1} = I_{o1}\left[\exp\left(\frac{V + IR_s}{\alpha_1 V_t}\right) - 1\right] \tag{7}$$

$$I_{d2} = I_{o2}\left[\exp\left(\frac{V + IR_s}{\alpha_2 V_t}\right) - 1\right] \tag{8}$$

where I_{o1} denotes to the diffusion current and I_{o2} refers to the saturation current. Furthermore, α_1 is the first diode ideality factor and α_2 is the second diode ideality factor.

Like SDM, the output current of the double diode model is given in Eq. (9), which is required to extract seven anonymous and uncertain parameters such as I_{o1}, I_{o2}, I_{ph} R_s, R_{sh}, α_1 and α_2.

$$I = I_{ph} - I_{o1}\left[\exp\left(\frac{V + IR_s}{\alpha_1 V_t}\right) - 1\right] - I_{o2}\left[\exp\left(\frac{V + IR_s}{\alpha_2 V_t}\right) - 1\right] - \frac{V + IR_s}{R_{sh}} \tag{9}$$

2.3. Photovoltaic module

As can be seen in Fig. 3, using several diodes which are connected either in series or in parallel, the relationship of voltage and the current can be acquired with the following formula for the photovoltaic module that is based on the SMM (Li et al., 2019a):

$$I = I_{ph}N_p - I_oN_p\left[\exp\left(\frac{V + IR_sN_s}{\alpha N_s V_t}\right) - 1\right] - \frac{V + IR_sN_s/N_p}{R_{sh}N_s/N_p} \tag{10}$$

where N_p refers to the number of solar cells connected in parallel and N_s is the number of solar cells connected in series. In this study, SMM is considered to be connected in series, thus N_p is equal to 1. Consequently, Eq. (10) can be changed based on the below formula,

$$I = I_{ph} - I_o\left[\exp\left(\frac{V + IR_sN_s}{\alpha N_s V_t}\right) - 1\right] - \frac{V + IR_sN_s}{R_{sh}N_s} \tag{11}$$

In SMM also, there exist five uncertain and anonymous parameters as (I_{ph}, I_o, R_s, R_{sh}, and α), which are required to be derived and extracted.

2.4. The cost function

Generally, in a realistic approach, parameter extraction problems are converted to optimization problems in which the optimization algorithms can be taken into account (Chen et al., 2019b, 2020; Ridha et al., 2021a; Wang et al., 2020b; Weng et al., 2021; Zhang et al., 2020k). Like the study conducted in Abbassi et al. (2019) and Qais et al. (2019b), the root mean square error (RMSE) has utilized as an objective function described as below in detail:

$$RMSE = \sqrt{\frac{1}{M}\sum_{m=1}^{M} f(V_m, I_m, x)^2} \tag{12}$$

where M is the amount of estimated I–V dataset, and x is regarded as a vector for measuring the extracted parameters. Thus, for various photovoltaic models, the objective functions are shown in Table 1.

3. Gradient-based optimizer (GBO)

GBO, a novel optimizer with stochastic and population strategy, is presented by Ahmadianfar et al. (2020a). This algorithm uses the logic of Newton's method to search in the solution space (Özban, 2004). The leading operators of the GBO are (1) gradient search rule (GSR) and (2) local escaping operator (LEO). In the following section, the main stages of the GBO are expressed.

3.1. Initialization

GBO uses N vectors in a d-dimensional search space as the population. In this algorithm, the initial population are randomly generated by using the following equations,

$$X_i = Low + rand \times (Up - Low) \tag{13}$$

where X_i refers to the ith vector, Low and Up are lower and upper bound of the solution space in each problem. *rand* denotes a rand number in the range of [0, 1].

3.2. Gradient search rule (GSR)

In the GBO, the GSR moves vectors toward a better position and explores the promising regions in the solution space. The GSR is based on Newton's method presented by Özban (2004). Therefore, the GSR is defined as,

$$GSR = randn \times \frac{2\Delta x \times x_i}{(y1_i - y2_i + \varepsilon)} \tag{14}$$

in which

$$y1_i = rand \times \left(\frac{[u_{i+1} + x_i]}{2} + rand \times \Delta x\right) \tag{14-1}$$

$$y2_i = rand \times \left(\frac{[u_{i+1} + x_i]}{2} - rand \times \Delta x\right) \tag{14-2}$$

and

$$u_{i+1} = x_i - randn \times \frac{2\Delta x \times x_i}{(x_{\text{worst}} - x_{\text{best}} + \varepsilon)} + DM \tag{15}$$

where u_{i+1} is the new solution generated in the GBO, *randn* is a random number with a normal distribution, x_{worst} and x_{best} and denote the worst and best solutions obtained during the optimization process, and ε denotes a number with a small value in the range of [0, 0.1]. *DM* denotes a direction movement, which is formulated as,

$$DM = rand \times F_2 \times (x_{best} - x_i^{it}) \tag{15-1}$$

where F_2 is an adaptive parameter, *it* is the iteration number. Δx refers to the difference between two vectors, which is defined as,

$$\Delta x = rand \times |\chi| \tag{15-2}$$

$$\chi = \frac{(x_{best} - x_{a1}^{it}) + \eta}{2} \tag{15-3}$$

$$\eta = 2 \times rand \times \left(\left|\frac{x_{a1}^{it} + x_{a2}^{it} + x_{a3}^{it} + x_{a4}^{it}}{4} - x_i^{it}\right|\right) \tag{15-4}$$

where $a1, a2, a3$, and $a4$ ($a1 \neq a2 \neq a3 \neq a4 \neq i$) are integers randomly chosen from [1, *N*], and, χ denotes the step size.

3.3. Generate new solutions

GBO employs the *GSR* and *DM* to create a new solution in each iteration of the optimization process. Therefore, the new solution ($Xnew1_i^{it}$) can be calculated as,

$$Xnew1_i^{it} = x_i^{it} - GSR + DM \tag{16}$$

$$Xnew1_i^{it} = x_i^{it} - randn \times F_1 \times randn \times \frac{2\Delta x \times x_i^{it}}{(y1_i - y2_i + \varepsilon)} + DM \tag{16-1}$$

in which
where F_1 and F_2 are two adaptive scale factors. These factors are employed to balance the exploration and exploitation and explore the promising regions in the search space, which are defined as,

$$F_1 = 2 \times rand \times \sigma - \sigma \tag{16-2}$$

$$F_2 = 2 \times rand \times \sigma - \sigma \tag{16-3}$$

$$\sigma = \left|\gamma \times \sin\left(\frac{3\pi}{2} + \sin\left(\alpha \times \frac{3\pi}{2}\right)\right)\right| \tag{16-4}$$

$$\gamma = \gamma_{min} + (\gamma_{max} - \gamma_{min}) \times \left(1 - \left(\frac{it}{MaxIt}\right)^3\right)^2 \tag{16-5}$$

where γ_{min} and γ_{max} are the minimum and maximum values of γ, which are determined by the user. *MaxIt* denotes the maximum number of iterations.

GBO uses another solution to increase the local search. To create this solution, the best-so-far solution has an important role. In this regard, the solution can be calculated as,

$$Xnew2_i^{it} = x_{\text{best}} - randn \times F_1 \times \frac{2\Delta x \times x_m^{it}}{(y1_i^{it} - y2_i^{it} + \varepsilon)} + rand \times F_2 \times (x_{a1}^{it} - x_{a2}^{it}) \tag{17}$$

Consequently, based on the solutions $Xnew1_i^{it}$ and $Xnew2_i^{it}$, the solution at the next iteration (x_i^{it+1}) is defined as:

$$x_i^{it+1} = r_1 \times \left(r_2 \times Xnew1_i^{it} + (1 - r_2) \times Xnew2_i^{it}\right) + (1 - r_1) \times Xnew3_i^{it} \tag{18}$$

in which

$$Xnew3_i^{it} = x_i^{it} - F_1 \times (Xnew2_i^{it} - Xnew1_i^{it}) \tag{18-1}$$

where r_1 and r_2 are two random numbers in the range of [0, 1].

3.4. Local escaping operator (LEO)

LEO is used in the GBO to increase the ability to escape the local solutions. According to this operator, a suitable solution (X_{LEO}^{it}) can be created concerning the condition $rand < 0.5$. To create this solution, the solutions x_{best}, $Xnew1_i^{it}$, $Xnew1_i^{it}$, x_{a1}^{it}, and x_{a2}^{it} have an essential role.

```
if rand < 0.5
  if rand < 0.5
    X_LEO^it = X_i^(it+1) + XL
  else
    X_LEO^it = x_best + XL
  end
  X_i^(it+1) = X_LEO^it
end
```
(19)

$$XL = \mu_1 \times \left(\vartheta_1 \times x_{\text{best}} - \vartheta_2 \times x_r^{it}\right) + \mu_2 \times F_1 \times \left(\vartheta_3 \times \left(Xnew2_m^{it} - Xnew1_m^{it}\right) + \vartheta_2 \times (x_{a1}^{it} - x_{a2}^{it})\right)/2 \tag{19-1}$$

where μ_1 and μ_2 are two random numbers in the range of [−1,1], and ϑ_1, ϑ_2, and ϑ_3 are three random values, which are described as:

$$\vartheta_1 = \begin{cases} 2 \times rand & if\ rand_1 < 0.5 \\ 1 & otherwise \end{cases} \tag{19-2}$$

$$\vartheta_2 = \begin{cases} rand & if\ rand_1 < 0.5 \\ 1 & otherwise \end{cases} \tag{19-3}$$

$$\vartheta_3 = \begin{cases} rand & if\ rand_1 < 0.5 \\ 1 & otherwise \end{cases} \tag{19-4}$$

where $rand_1$ is a number in the range of [0, 1].

To specified the solution x_r^{it} in Eq. (19-1), the following scheme is defined.

$$x_r^{it} = \begin{cases} x_p & if\ rand_2 < 0.5 \\ x_p^{it} & otherwise \end{cases} \tag{19-5}$$

$$x_p = U + rand \times (U - L) \tag{19-6}$$

where x_p is a random solution, x_p^{it} is a randomly selected solution ($p \in [1, 2, \ldots, N]$), and $rand_2$ is a random number in the range of [0, 1].

Table 2
Pseudocode of the EGBO.

Initialization: Control parameter: $MaxIt$ and $LC = 0.7$
Form the initial population as well as assess objective functions
for $it = 1$ to $MaxIt$
  Sort population in ascending order
  for $i = 1$ to N
    Produce F_1, F_2 using Eq. (20) and pc_r using Eqs. (21-1)
  End
  for $i = 1 : N$
    Select randomly $a1 \neq a2 \neq a3 \neq a4 \neq i$ in the range of $[1, N]$
    Generate the positions $Xnew1_i^{it}$ and $Xnew1_i^{it}$ using Eqs. (16) and (17) respectively;
    Implement crossover operator using Eq. (21)
    $LC = 4 \times LC \times (1\text{-}LC)$
    if $rand < LC$
      Implement MLEO using Eqs. (22)–(23)
    End
    if $f(Xnew) < f(x_i^{it})$
      $x_i^{it+1} = Xnew$
    Else
      $x_i^{it+1} = x_i^{it}$
    End
  End
Update x_{best}, x_{best2}, x_{best3}, and x_{worst}
$it = it+1$
end
Output: x_{best}

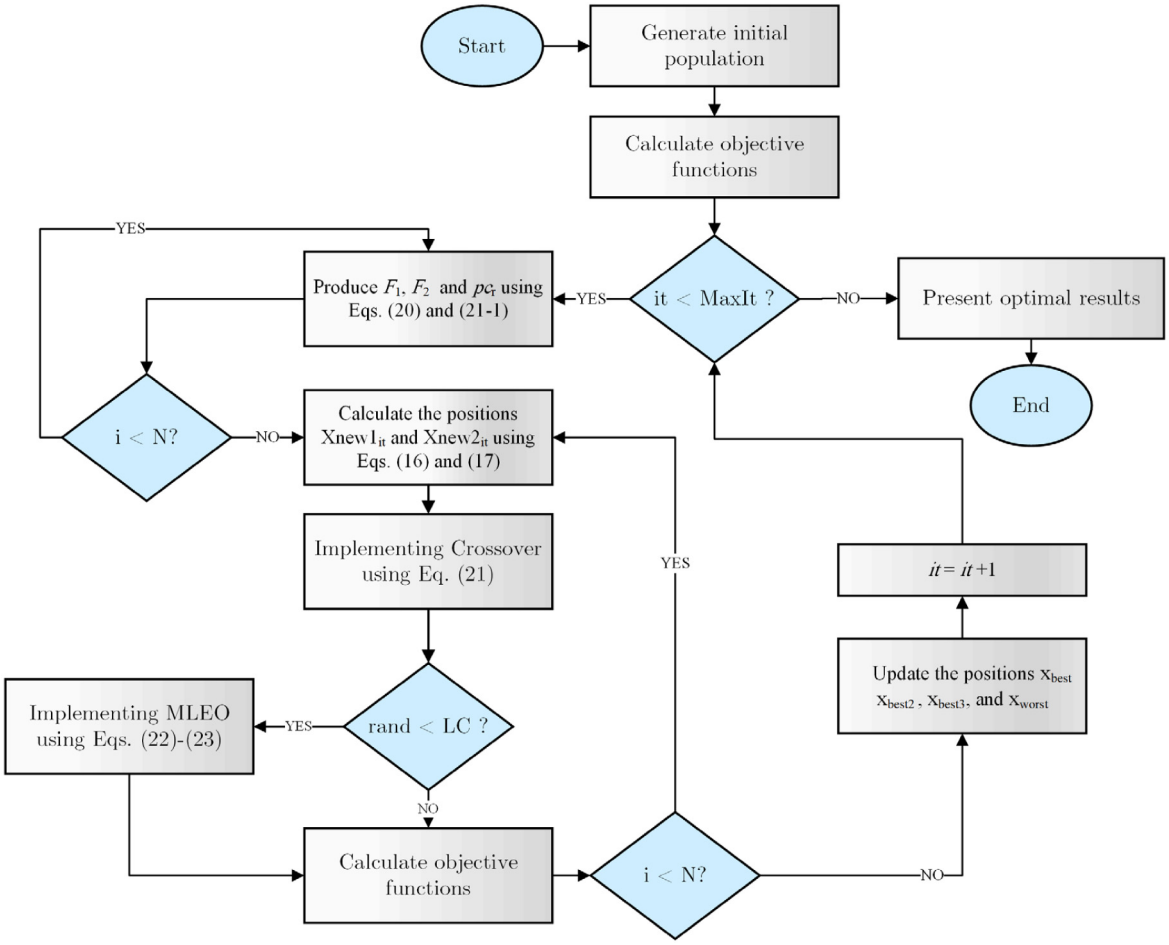

Fig. 4. Flowchart of the EGBO algorithm.

4. Enhanced gradient-based optimizer (EGBO)

In this study, an enhanced gradient-based optimizer (EGBO) is introduced to extract different PV models' parameters accurately. The main motives for enhancing the original GBO are described in the following sections.

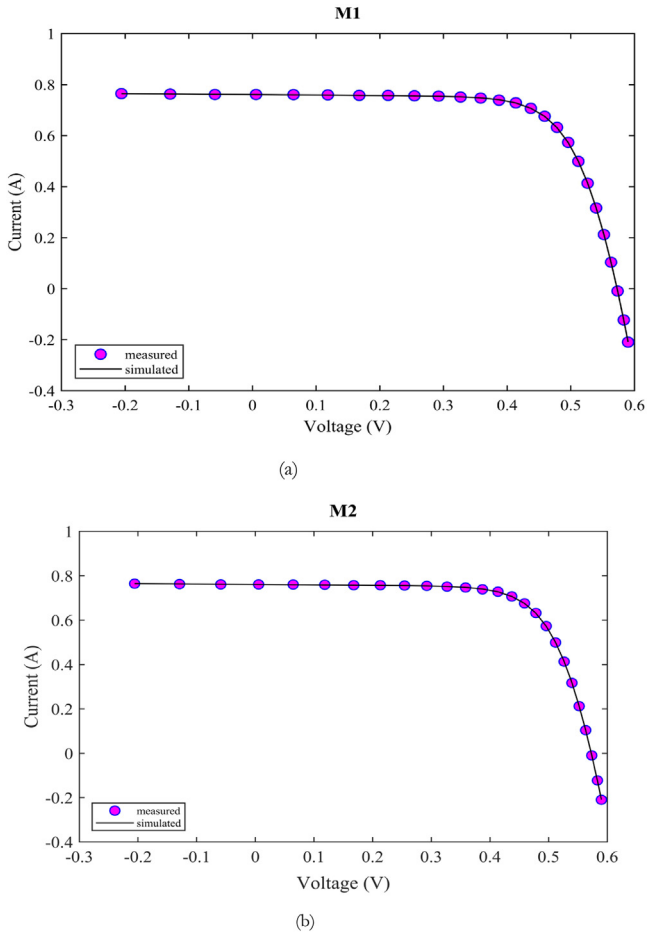

Fig. 5. Comparison between the I–V curves simulated by the EGBO versus measured data: EGBO: (a) M1, (b) M2.

Table 3
Lower (L) and upper (U) bound of each parameter for each PV model.

Parameter	M1/M2		M3		M4		M5	
	L	U	L	U	L	U	L	U
I_{ph} (A)	0	1	0	2	0	2	0	8
I_o, I_{o1}, I_{o2} (μA)	0	1	0	50	0	50	0	50
R_s (Ω)	0	0.5	0	2	0	0.36	0	0.36
R_{sh} (Ω)	0	100	0	2000	0	1000	0	1500
α, α_1, α_2	1	2	1	50	1	60	1	50

Table 4
Values of control parameters for all optimizers.

Optimizer	Value of control parameter
SaDE	$N = 50$
jDE	$N = 50$, $F_l = 0.1$, $F_u = 0.9$, $\tau_1 = \tau_2 = 0.1$
SDE	$N = 50$
AGDE	$N = 50$
SHADE	$N = 50$, $H = 10$
EJADE	$N_{min} = 4$, $N_{max} = 50$
ITLBO	$N = 50$
JADE	$N = 50$
EGBO	$N = 50$

4.1. The proposed mechanism to update parameters

In the GBO, proper specifying two parameters F_1 and F_2 has an essential role in increasing precision and convergence speed. In this study, these parameters are determined by the introduced mechanism by Tang et al. (2014). According to Tang et al. (2014) and Ahmadianfar et al. (2020b), small values of control parameters are relatively allocated to the superior solutions, while large values are assigned to the inferior solutions. To do this, a rank-based mechanism is used so that all the individuals are first sorted in ascending order based on their objective functions' values. After that, the following scheme is used to formulate these parameters.

$$\begin{aligned}
&\textbf{if } rand < 0.5\\
&\quad F_1 = a1/N + 0.1 \times randn\\
&\quad F_2 = a2/N + 0.1 \times randn\\
&\textbf{else}\\
&\quad F_1 = i/N + 0.1 \times randn\\
&\quad F_2 = i/N + 0.1 \times randn\\
&\textbf{end}
\end{aligned} \tag{20}$$

where a_1 and a_2 are two random integer numbers in the range of $[1, N]$.

4.2. The crossover operator

In this study, to enhance the population diversity, the crossover operator is applied by combining the solutions $Xnew1_j$ and $Xnew2_j$ generated by the GBO with the current solution $(x_{i,j})$ as follows:

$$\begin{aligned}
&\textbf{for } j = 1 \text{ to } d\\
&\quad \textbf{if } rand < pc_r \text{ or } j = j_{rand}\\
&\quad\quad \textbf{if } rand < 0.5\\
&\quad\quad\quad Xnew_j = Xnew1_j\\
&\quad\quad \textbf{else}\\
&\quad\quad\quad Xnew_j = Xnew2_j\\
&\quad\quad \textbf{end}\\
&\quad \textbf{else}\\
&\quad\quad Xnew_j = x_{i,j}\\
&\quad \textbf{end}\\
&\textbf{end}
\end{aligned} \tag{21}$$

where pc_r denotes the crossover probability rate. Similar to the previous section, to determine the pc_r, all the members of the population are sorted in ascending order based on the objective function values. j_{rand} denotes an integer randomly number in the range of [1, D]. pc_r is defined based on the following equation,

$$C_r = i/N + 0.1 \times randn \tag{21-1}$$

4.3. The modified local escaping operator (MLEO)

In this section, a modified version of the LEO (MLEO) is developed to promote the original LEO's performance. The proposed

Table 5
Comparison different optimizers on M1.

Algorithm	I_{ph} (A)	I_o (μA)	R_s (Ω)	R_{sh} (Ω)	a	RMSE
JADE	0.7608	3.23E−07	0.0364	53.6477	1.4811	9.8602E−04
jDE	0.7607	3.27E−07	0.0363	53.8083	1.4824	9.8602E−04
SaDE	0.7607	3.23E−07	0.0363	53.7179	1.4811	9.8602E−04
AGDE	0.7607	3.23E−07	0.0363	53.7187	1.4811	9.8602E−04
SHADE	0.7607	3.23E−07	0.0363	53.7173	1.4811	9.8744E−04
SDE	0.7607	3.23E−07	0.0363	53.7203	1.4811	9.8602E−04
ITLBO	0.7607	3.23E−07	0.0363	53.7185	1.4811	9.8602E−04
EJADE	0.7607	3.23E−07	0.0363	53.7185	1.4811	9.8602E−04
EGBO	0.7608	3.23E−07	0.0364	53.7185	1.4811	9.8602E−04

Table 6
Comparison of different optimizers on M2.

Algorithm	I_{ph} (A)	I_{o1} (μA)	R_s (Ω)	R_{sh} (Ω)	a_1	I_{o2} (μA)	a_2	RMSE
JADE	0.7607	2.59E−07	0.0365	54.6356	1.4630	3.3E−07	1.9039	9.8395E−04
jDE	0.7608	4.78E−09	0.0363	53.8999	1.8369	3.26E−07	1.4823	9.8667E−04
SaDE	0.7607	3.21E−07	0.0363	53.5995	1.4805	2.39E−09	1.7519	9.8640E−04
AGDE	0.7607	7.05E−07	0.0367	55.0120	1.9996	2.28E−07	1.4515	9.8331E−04
SHADE	0.7606	2.76E−07	0.0363	55.8990	1.4698	2.06E−07	1.8130	9.9013E−04
SDE	0.7607	5.61E−08	0.0362	53.9079	1.8958	3.18E−07	1.4804	9.9100E−04
ITLBO	0.7607	2.17E−07	0.0367	55.6940	1.4477	8.26E−07	1.9999	9.8253E−04
EJADE	0.7608	2.25E−07	0.0367	55.4854	1.4510	7.49E−07	2.0000	**9.8248E−04**
EGBO	0.7608	2.25E−07	0.0367	55.4855	1.4510	7.49E−07	2.0000	**9.8248E−04**

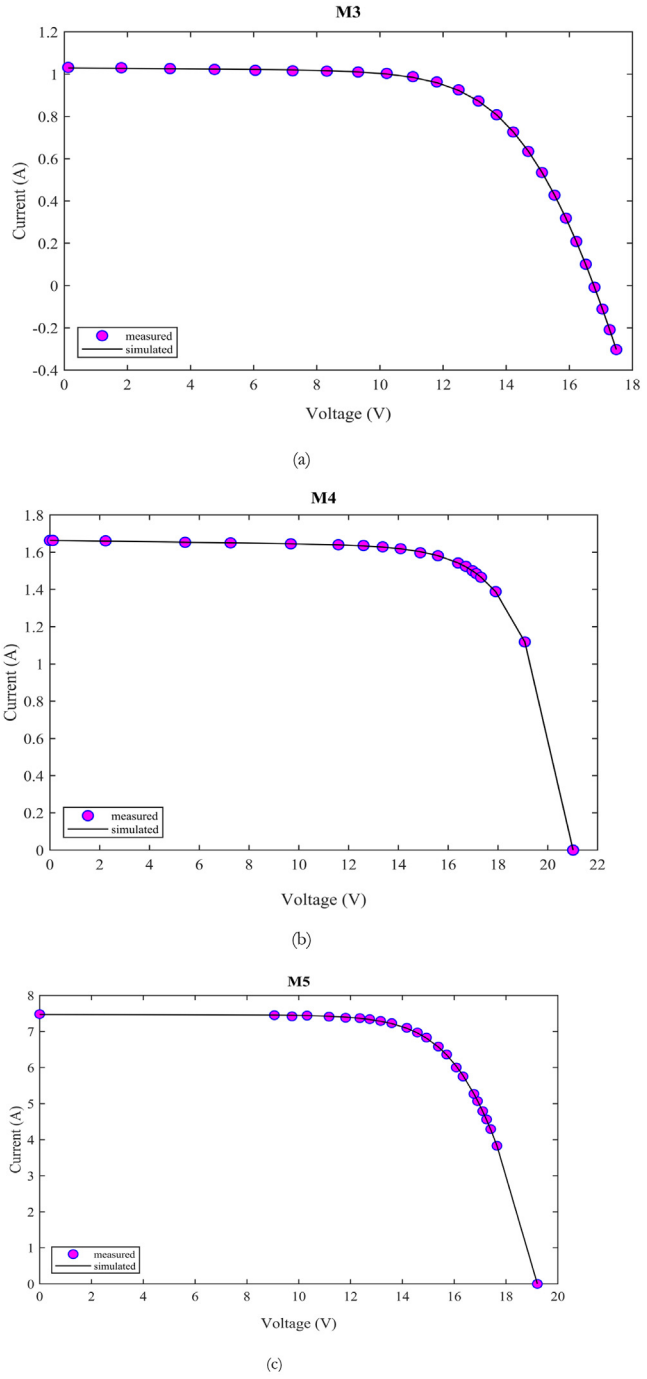

Fig. 6. Comparison between the I–V curves simulated by the EGBO versus measured data: (a) M3, (b) M4, (c) M5.

Table 7
Comparison of different optimizers on M3.

Algorithm	I_{ph} (A)	I_o (μA)	R_s (Ω)	R_{sh} (Ω)	a	RMSE
JADE	1.0305	3.48E−06	1.2012	981.9823	48.6428	2.4251E−03
jDE	1.0305	3.48E−06	1.2012	981.9823	48.6428	2.4251E−03
SaDE	1.0305	3.48E−06	1.2012	981.8990	48.6425	2.4251E−03
AGDE	1.0305	3.48E−06	1.2012	981.9824	48.6428	2.4251E−03
SHADE	1.0305	3.48E−06	1.2012	981.9454	48.6426	2.4251E−03
SDE	1.0305	3.48E−06	1.2013	982.4560	48.6412	2.4251E−03
ITLBO	1.0305	3.48E−06	1.2013	981.9824	48.6428	2.4251E−03
EJADE	1.0305	3.48E−06	1.2012	981.9823	48.6428	2.4251E−03
EGBO	1.0305	3.48E−06	1.2013	981.9822	48.6428	2.4251E−03

Table 8
Comparison of different optimizers on M4.

Algorithm	I_{ph} (A)	I_o (μA)	R_s (Ω)	R_{sh} (Ω)	a	RMSE
JADE	1.6638	1.79E−06	0.0041	16.0270	1.5232	1.7310E−03
jDE	1.6625	3.05E−06	0.0023	19.1595	1.5847	2.1900E−03
SaDE	1.6623	2.58E−06	0.0030	18.8899	1.5649	1.9839E−03
AGDE	1.6637	1.88E−06	0.0040	16.3499	1.5292	1.7442E−03
SHADE	1.6631	2.2E−06	0.0035	17.4160	1.5464	1.8189E−03
SDE	1.6620	3.94E−06	0.0014	21.608	1.6160	2.6202E−03
ITLBO	1.6638	1.77E−06	0.0042	15.9672	1.5221	1.7308E−03
EJADE	1.6639	1.74E−06	0.0042	15.9282	1.5203	**1.7298E−03**
EGBO	1.6639	1.73E−06	0.0043	15.9283	1.5203	**1.7298E−03**

Table 9
Comparison of different optimizers on M5.

Algorithm	I_{ph} (A)	I_o (μA)	R_s (Ω)	R_{sh} (Ω)	a	RMSE
JADE	7.4718	2.42E−06	0.0045	24.7295	1.2632	1.6608E−02
jDE	7.4802	6.28E−06	0.0040	1454.97	1.3487	2.2478E−02
SaDE	7.4620	2.83E−0	0.0045	522.506	1.2764	1.6842E−02
AGDE	7.4627	2.71E−06	0.0045	153.329	1.2726	1.6773E−02
SHADE	7.4633	2.94E−06	0.0044	1031.17	1.2796	1.6894E−02
SDE	7.4611	2.68E−06	0.0045	209.244	1.2715	1.6777E−02
ITLBO	7.4719	2.43E−06	0.0045	24.4940	1.2635	**1.6601E−02**
EJADE	7.4725	2.33E−06	0.0046	22.2199	1.2601	**1.6601E−02**
EGBO	7.4725	2.33E−06	0.0046	22.2199	1.2601	**1.6601E−02**

MLEO is expressed in the following scheme:

if $rand < LC$

$$\textit{if } rand < 0.5 \times \left(1 - \frac{it}{MaxIt}\right)$$

$$Xnew = x_{best3} + F_1 \times \left(x_{best2} - x_r^{it}\right) + F_2 \times \left(x_{a1}^{it} - x_{a2}^{it}\right) \quad (22)$$

else

$$Xnew = x_{best} + F_1 \times \left(x_{best2} - x_r^{it}\right) + F_2 \times \left(x_{a1}^{it} - x_{a2}^{it}\right) \quad (23)$$

end

end

where LC is a chaotic logistic map ($LC = 4 \times \mathrm{LC} \times (1 - LC)$). The initial value of LC is equal to 0.7. Based on the MLEO, the EGBO uses Eq. (22) to create the new solution ($Xnew$) in the initial iterations and then in the last iterations, and it tends to use Eq. (23) according to the condition $rand < 0.5 \times \left(1 - \frac{it}{MaxIt}\right)$.

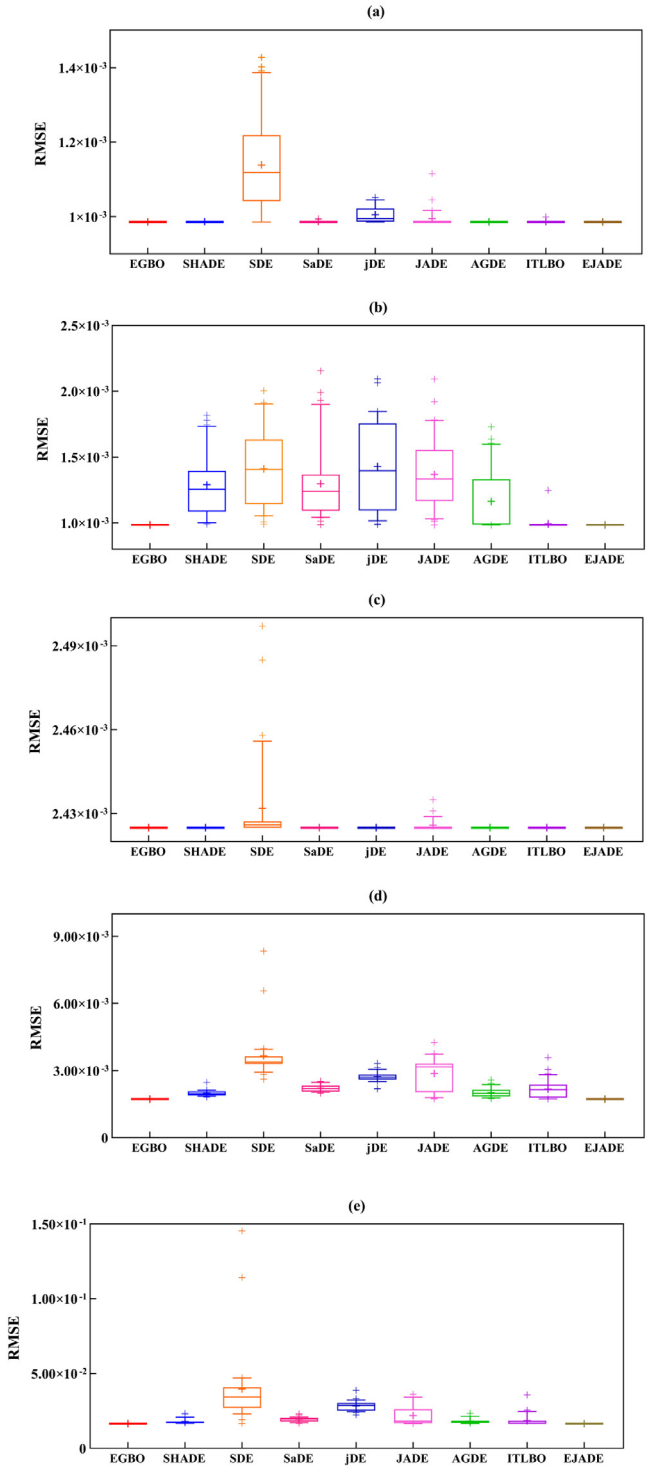

Fig. 7. Boxplot of RMSE over 30 different runs of all optimization algorithms for (a) M1, (b) M2, (c) M3, (d) M4, and (e) M5.

x_{best2} and x_{best3} are the second and third-best-so-far solutions over the optimization process. Table 2 presents the pseudocode of the EGBO algorithm. Fig. 4 demonstrates the flowchart of the EGBO algorithm. It should be noted that the computational complexity of the EGBO can be calculated based on its four components, including the initialization, evaluation of objective function, control parameters (i.e., F_1 and F_2) update, and solution update. The complexity of initialization is O(N), the complexity of objective function evaluation and sorting is O(N+Nlog$N$), the complexity of updating control parameters is O($N\times D$), and the complexity of updating solutions is O($N\times D$). Accordingly, the computation complexity of EGBO is equal to O($N\times$(1+$it\times$N$\times$(1+log$N$+2$\times N$).

5. Results and analysis

For performance evaluation of the developed EGBO, different photovoltaic models' parameters are required to be extracted, i.e., SDM (M1), DDM (M2), and SMM (M3–M5). We have performed the tests based on principals of fair comparison (Ahmadianfar et al., 2021; Li et al., 2019b; Zhang et al., 2021b; Chen et al., 2021).

In these tests, the benchmark I–V features and characteristic of solar cells' two cases concerning the single diode model (Ns = Np = 1) and the double diode model (Ns = 1, Np = 2), have been calculated at a 57 mm diameter commercial R.T.C France silicon cell at 33 °C, consisting of 26 pairs of current and voltage values (Easwarakhanthan et al., 1986).

There are three photovoltaic module models in the SMM, which include Photowatt-PWP201 (M3), mono-crystalline STM6-40/36 (M4), and poly-crystalline STP6-120/36 (M5). The M3 module data, estimated under 1000 W/m2 at 45 °C, has been acquired from Easwarakhanthan et al. (1986). On the other hand, the data of mono-crystalline M4 obtained from Tong and Pora (2016) is measured at 51 °C, and the data of poly-crystalline M5 has been acquired from Gao et al. (2018) is measured at 55 °C. Thirty-six cells are connected in series in these PV module models. Table 3 gives the ranges of each PV model's parameters, which are the same as the previous literature (Chen et al., 2016). Note that in all the modules, the maximum evaluation number (MaxNFE) is set to be 2.00E+05 for EGBO's input parameter. Moreover, each algorithm has been performed over 30 independent runs.

Additionally, to validate the superiority of the developed EGBO, we have compared it with eight state-of-the-art algorithms such as SaDE (Qin and Suganthan, 2005), SDE (Omran et al., 2005), JADE, AGDE (Mohamed and Mohamed, 2019), jDE, SHADE (Tanabe and Fukunaga, 2013), EJADE (Li et al., 2020b), and ITLBO. The parameters of the abovementioned algorithms are available in Table 4.

5.1. Results on single diode model

The RMSE values and the related attained parameters for the M1 are reported in Table 5. Note that the best-obtained results are marked in **boldface** only when the RMSE value is minimal. As shown in Table 5, EGBO, SaDE, SDE, jDE, JADE, EJADE, ITLBO, and AGDE algorithms have acquired the best RMSE value that is 9.8602E−04, and RMSE value is 9.8744E−04 in the SHADE. Due to the unavailability of information about the accurate parameter values, the RMSE has been utilized to imply accuracy. In addition, to reconstruct the simulated I–V data, I–V character curves were plotted using the extracted EJADE parameter values and compared with the surveyed data, as shown in Fig. 5(a). From I–V curves, it is clear that the simulated and measured data are highly coincided and compatible with each other; moreover, the extracted parameters of EJADE are very precise and accurate.

5.2. Results on double diode model

According to sub Section 2.2, in M2, there exist several unknown parameters to be extracted. This issue is required to be addressed to solve the problems of parameter extraction. At this moment, EGBO has been employed in M2. The comparison results of seven parameter extraction optimizers are available in Table 6. As observed from Table 6, all algorithms have slightly different

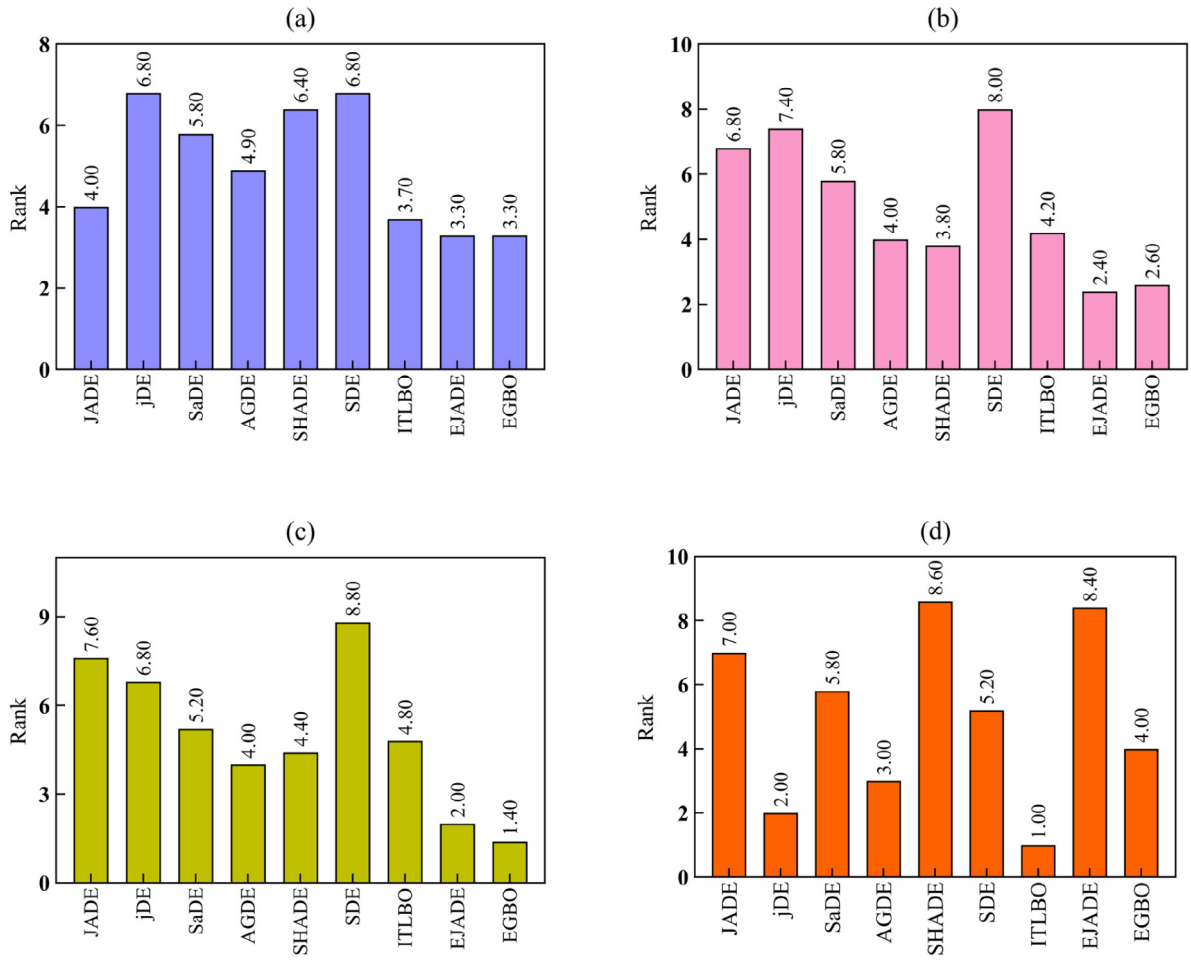

Fig. 8. Friedman ranks of all optimizers for (a) min, (b) mean, (c) SD, and (d) CPU time of RMSE over 30 runs for five models.

RMSE values by increasing the parameter extraction complexity except EGBO and EJADE, which reached the best RMSE value (9.824E−04). These two methods' extracted parameters are remarkably consistent, while the performance of SHADE (RMSE = 9.9013E−04) and SDE (RMSE = 9.9100E−04) is not satisfactory. A plus point is that although JADE, jDE, SaDE, AGDE, and ITLBO reached the optimal results in M1, they do not gain the optimal RMSE value in M2. Furthermore, as shown in Fig. 5(b), for verifying the accuracy of extracted parameters of EGBO like M1, the *I-V* curves have been provided among measured and simulated data, and the simulated and measured data are also highly coherent.

5.3. Results on photovoltaic module model

The relevant parameter extraction results in M1 and M2 are explained in detail in Sections 5.1 and 5.2. In particular, for M2, the performance analysis of EGBO and EJADE outweigh other algorithms' performance. In this section, the optimal parameters and RMSE values have been summarized in Tables 7–9 for the SMM modules (i.e., Photowatt-PWP201, STM6-40/36, and STP6-120/36), which all optimizers have extracted. As it is evident, all the optimizers can reach the same RMSE value (2.4251E−03) for the M3 (Table 7). Form Table 8, we can see that EGBO and EJADE have obtained the best RMSE value for the M4 module (RMSE = 1.7298E−03). Moreover, as observed from Table 9, EGBO, JADE, and ITLBO obtained the best RMSE value for the M5 modules (RMSE = 1.6601E−02) optimizers like JADE, jDE, SaDE, AGDE, SHADE, and SDE did not. Moreover, to evaluate the precision of parameter values derived by EGBO, the I–V curves simulated data versus measured data are displayed in Fig. 6, where the simulated results obtained by EGBO are also very compatible with the measured data.

5.4. Statistical results and convergence speed

Based on the subsections mentioned above, the developed EGBO algorithm has shown great computational accuracy and efficiency comparing with several well-known optimizers available in the literature. Additionally, for confirming the promising performance of the EGBO, some metrics are applied, where 30 independent runs have applied minimum (Min), maximum (Max), the average value (Mean), standard deviation (SD), the Friedman rank test, and total CPU time. Table 10 represents the statistical results, and the conclusions are as below:

All the optimizers may give the best RMSE values for M1 and M3 modules corresponding to the Min RMSE values.

Based on the Min RMSE obtained values in M4 and M2, only EGBO and EJADE can reach the best results. Moreover, concerning the values of Min RMSE in the M5 module, the EGBO, EJADE, and ITLBO can obtain the best results.

Additionally, the results' distribution obtained from various optimization algorithms based on 30 runs is depicted in Fig. 7. Consider that in Fig. 7, the symbol "+" refers to the outlier when plotting the boxplot. Accurate and reliable performance analysis of the developed EGBO has been validated by examining the solution distribution span.

Based on Fig. 8, the EJADE has the best rank values in the Mean (2.4) term, followed by the EGBO with the rank of 2.6

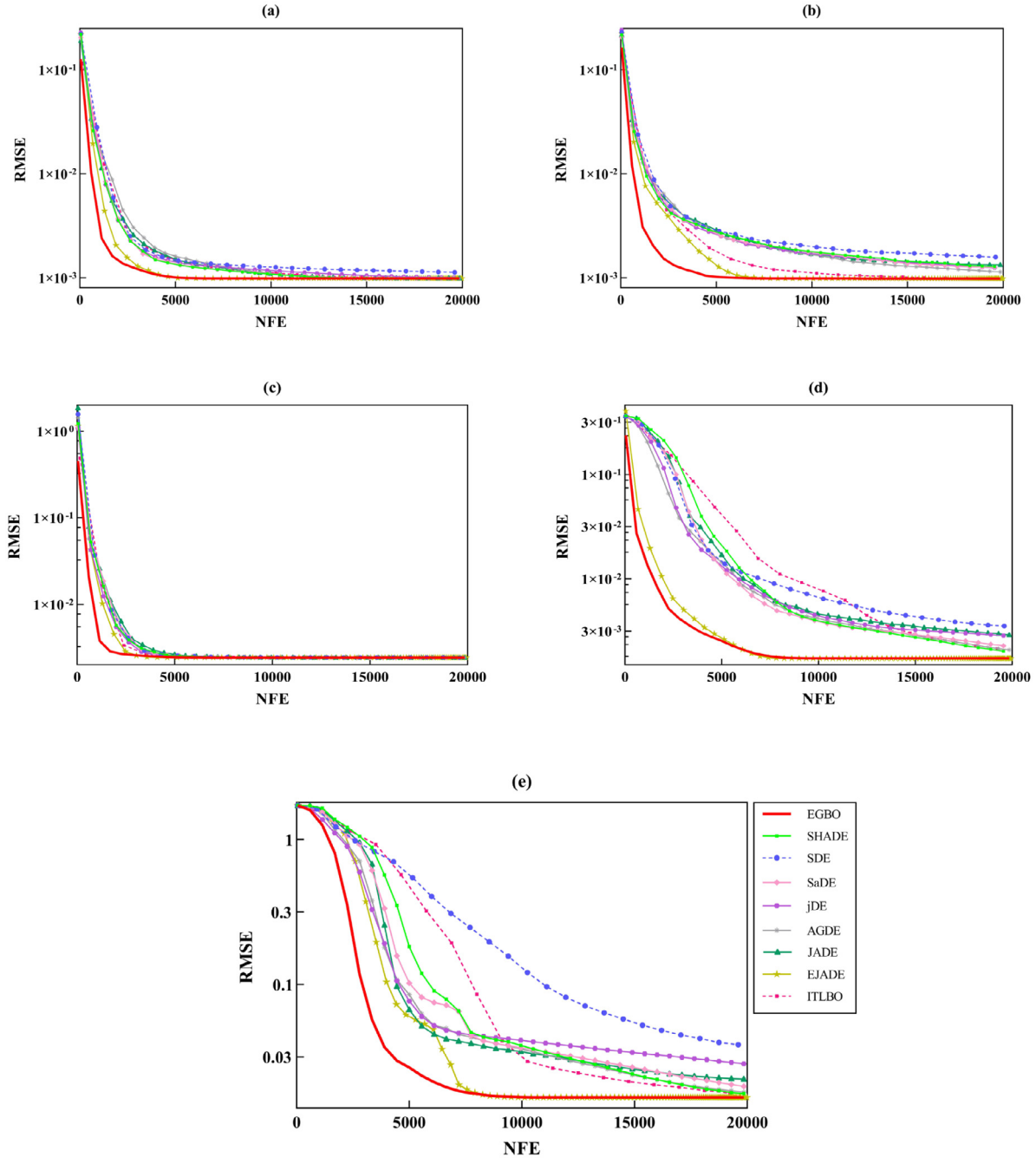

Fig. 9. Convergence curves of all optimizers for (a) M1, (b) M2, (c) M3, (d) M4, and (e) M5.

concerning the Freidman rank test. Admittedly, these optimization algorithms have similar performances. Moreover, EGBO's efficiency is favorable in terms of the SD with the rank of 1.4 and CPU with the rank of 4. Regarding the obtained results, the CPU processing time for EJADE is more than the CPU time for the EGBO (about twice). It is apparent that EGBO faster than EJADE for solving the photovoltaic modules. The EGBO is more promising and reliable compared with other algorithms concerning the SD values. To make it clear, the extracted parameters obtained from the EGBO algorithm are more reliable and accurate.

Regarding the CPU time, ITLBO, jDE, AGDE, and EGBO are the fastest methods for 30 independent runs, followed by SDE, SaDE, JADE, EJADE, and SHADE. Although the EGBO is not the fastest optimizer, it is still satisfactory and favorable compared to SDE, SaDE, JADE, EJADE, and SHADE.

EJADE, ITLBO, AGDE, and SHADE are the most competitive algorithms to the developed EGBO based on the performance analysis and statistical results. Therefore, we have performed more experimental analyses for investigating the convergence of the abovementioned techniques. In all of these optimizers, the MaxNFE is chosen to be equal to 20,000. Fig. 9 indicates the convergence curves, and it is evident that EGBO and EJADE are the fastest models, particularly for M1, M4, and M5. According to this figure, in addition to the fact that EGBO has a better convergence speed in the initial iteration, it also performs more accurately than the other methods. This performance is due to the proposed MLEO can assist in escaping from local solutions, and a novel mechanism to update the control parameters can efficiently improve accuracy and convergence speed. In addition, ITLBO, SHADE, and SDE have a poor convergence rate, especially

Table 10
Statistical results of M1 to M5 for different optimizers.

Model	RMSE					CPU time (s)
		Min	Max	Mean	SD	
M1	JADE	9.8602E−04	1.1161E−03	9.9500E−04	2.62E−05	23.00
	jDE	9.8602E−04	1.0519E−03	1.0052E−03	2.17E−05	6.88
	SaDE	9.8602E−04	9.9398E−04	9.8661E−04	1.87E−06	16.00
	AGDE	9.8602E−04	9.8602E−04	**9.8602E−04**	2.79E−10	8.39
	SHADE	9.8602E−04	9.8655E−04	9.8603E−04	9.56E−08	23.55
	SDE	9.8602E−04	1.4268E−03	1.1387E−03	1.29E−04	15.05
	ITLBO	9.8602E−04	9.9926E−04	9.8646E−04	2.42E−06	3.06
	EJADE	9.8602E−04	9.8602E−04	**9.8602E−04**	4.36E−17	23.01
	EGBO	9.8602E−04	9.8602E−04	**9.8602E−04**	**3.33E−17**	13.18
M2	JADE	9.8395E−04	2.0929E−03	1.3693E−03	2.70E−04	23.97
	jDE	9.8667E−04	2.0938E−03	1.4277E−03	3.44E−04	8.20
	SaDE	9.8640E−04	2.1551E−03	1.2981E−03	2.91E−04	15.54
	AGDE	9.8331E−04	1.7304E−03	1.1633E−03	2.39E−04	8.73
	SHADE	9.9013E−04	1.8182E−03	1.2892E−03	2.41E−04	24.95
	SDE	9.9100E−04	2.0055E−03	1.4110E−03	2.94E−04	15.50
	ITLBO	9.8253E−04	1.2491E−03	9.9391E−04	4.82E−05	3.03
	EJADE	9.8248E−04	9.8602E−04	**9.8437E−04**	**1.47E−06**	24.83
	EGBO	9.8248E−04	9.8681E−04	9.8484E−04	1.66E−06	13.49
M3	JADE	2.4251E−03	2.4350E−03	2.4259E−03	2.30E−06	21.14
	jDE	2.4251E−03	2.4251E−03	**2.4251E−03**	2.58E−11	7.34
	SaDE	2.4251E−03	2.4251E−03	**2.4251E−03**	6.91E−10	16.07
	AGDE	2.4251E−03	2.4251E−03	**2.4251E−03**	5.84E−15	8.95
	SHADE	2.4251E−03	2.4251E−03	**2.4251E−03**	3.38E−12	22.59
	SDE	2.4251E−03	2.4970E−03	2.4319E−03	1.74E−05	15.05
	ITLBO	2.4251E−03	2.4251E−03	**2.4251E−03**	**2.28E−17**	3.04
	EJADE	2.4251E−03	2.4251E−03	**2.4251E−03**	2.45E−17	24.14
	EGBO	2.4251E−03	2.4251E−03	**2.4251E−03**	2.38E−17	12.84
M4	JADE	1.7310E−03	4.2619E−03	2.8737E−03	7.20E−04	22.25
	jDE	2.1900E−03	3.3270E−03	2.7258E−03	2.36E−04	6.77
	SaDE	1.9839E−03	2.5323E−03	2.2194E−03	1.60E−04	15.64
	AGDE	1.7442E−03	2.5866E−03	2.0228E−03	2.11E−04	8.18
	SHADE	1.8189E−03	2.4831E−03	1.9879E−03	1.36E−04	25.16
	SDE	2.6202E−03	8.3489E−03	3.6623E−03	1.10E−03	15.91
	ITLBO	1.7308E−03	3.5858E−03	2.1750E−03	4.32E−04	3.10
	EJADE	1.7298E−03	1.7298E−03	**1.7298E−03**	9.67E−18	23.78
	EGBO	1.7298E−03	1.7298E−03	**1.7298E−03**	**8.22E−18**	13.18
M5	JADE	1.6608E−02	3.6371E−02	2.1878E−02	6.78E−03	21.58
	jDE	2.2478E−02	3.8862E−02	2.8388E−02	3.42E−03	6.92
	SaDE	1.6842E−02	2.3209E−02	1.9421E−02	1.52E−03	16.13
	AGDE	1.6773E−02	2.3382E−02	1.8145E−02	1.60E−03	8.43
	SHADE	1.6894E−02	2.3417E−02	1.7992E−02	1.70E−03	23.18
	SDE	1.6777E−02	1.4540E−01	3.9699E−02	2.61E−02	15.28
	ITLBO	1.6601E−02	3.5718E−02	1.8505E−02	4.02E−03	3.06
	EJADE	1.6601E−02	1.6601E−02	**1.6601E−02**	2.23E−16	24.01
	EGBO	1.6601E−02	1.6601E−02	**1.6601E−02**	**1.47E−16**	12.82

Table 11
Analysis of the basic GBO and EGBO for different PV models.

Model	Algorithm	RMSE				CPU time (s)
		Min	Max	Mean	SD	
M1	GBO	9.8602E−04	9.8632E−04	9.8603E−04	5.38E−08	32.12
	EGBO	9.8602E−04	9.8602E−04	9.8602E−04	2.83E−17	30.01
M2	GBO	9.8249E−04	1.4058E−03	1.0124E−03	1.02E−04	33.78
	EGBO	9.8248E−04	9.8681E−04	9.8484E−04	1.46E−06	32.73
M3	GBO	2.4251E−03	2.4251E−03	2.4251E−03	4.08E−09	31.12
	EGBO	2.4251E−03	2.4251E−03	2.4251E−03	2.79E−17	31.70
M4	GBO	1.7298E−03	2.0153E−03	1.7443E−03	5.30E−05	32.01
	EGBO	1.7298E−03	1.7298E−03	1.7298E−03	7.66E−18	29.50
M5	GBO	1.6601E−02	2.2642E−02	1.6855E−02	1.09E−03	30.91
	EGBO	1.6601E−02	1.6601E−02	1.6601E−02	1.19E−16	31.58

in the initial iterations. Thus, we will know that the developed EJADE algorithm can speed up, providing us with some more reliable parameter values.

In this research, all models are optimized using the GBO to demonstrate the proposed EGBO efficiency better. For two optimizers, the maximum number of NFE (MaxNFE) is equal to 50,000. Table 11 indicates the statistical results of the EGBO and GBO algorithms for five models. In comparison to the GBO, it can be seen that the EGBO encompasses a very notable improvement in terms of Min, Max, Mean, and SD. Also, the CPU time of the proposed EGBO in most models is less than the GBO algorithm. Finally, Fig. 10 illustrates the convergence curves of two optimizers (i.e., EGBO and GBO). To better illustrate convergence curves' variation over the optimization process, Fig. 10 displays based on

Table 12
Statistical results on case 1 at dissimilar irradiance and temperature of 25 °C.

Algorithm	200 W/m^2		400 W/m^2		600 W/m^2		800 W/m^2		1000 W/m^2	
	Mean	SD	Mean	SD	Mean	SD	Mean	SD	Mean	SD
JADE	8.5141E−03	5.32E−03	1.3329E−02	6.09E−03	1.7598E−02	1.59E−02	2.4954E−02	2.30E−02	3.2339E−02	2.90E−02
jDE	4.5539E−03	4.16E−04	1.3198E−02	7.50E−04	3.1260E−02	2.84E−03	4.8014E−02	4.12E−03	5.5593E−02	4.54E−03
SaDE	3.0474E−03	3.71E−04	7.9817E−03	8.32E−04	1.4274E−02	2.63E−03	2.2514E−02	3.64E−03	2.4954E−02	6.49E−03
AGDE	5.1901E−03	1.40E−03	1.1189E−02	2.80E−03	1.8521E−02	6.22E−03	3.0907E−02	9.95E−03	3.2044E−02	1.17E−02
SHADE	2.4058E−03	1.41E−04	5.7594E−03	5.44E−04	8.8058E−03	5.73E−04	1.5533E−02	1.39E−03	1.5099E−02	2.00E−03
SDE	1.2129E−02	2.63E−03	1.7928E−02	6.66E−04	4.6742E−02	4.24E−03	6.3793E−02	3.65E−03	7.2740E−02	7.30E−03
ITLBO	3.2746E−03	5.86E−04	6.8981E−03	1.13E−03	9.2799E−03	1.26E−03	1.5262E−02	2.15E−03	1.5021E−02	2.30E−03
EJADE	1.4185E−03	7.91E−18	1.4262E−03	4.67E−17	1.2977E−03	7.91E−17	1.6310E−03	1.04E−16	1.5390E−03	2.24E−16
EGBO	1.4185E−03	9.28E−18	1.4262E−03	**3.08E−17**	1.2977E−03	**5.79E−17**	1.6310E−03	1.75E−16	1.5390E−03	**1.97E−16**

Table 13
Statistical results on case 1 at different temperature and irradiance of 1000 W/m^2.

Algorithm	25 °C		50 °C		75 °C	
	Mean	SD	Mean	SD	Mean	SD
JADE	2.3502E−02	2.52E−02	2.2876E−02	2.55E−02	1.1093E−02	1.21E−02
jDE	5.3336E−02	4.28E−03	3.6137E−02	4.00E−03	1.8166E−02	4.09E−03
SaDE	2.6695E−02	5.60E−03	8.5435E−03	2.27E−03	5.2526E−03	1.01E−03
AGDE	3.2869E−02	1.19E−02	1.2427E−02	9.21E−03	5.1528E−03	1.97E−03
SHADE	1.5537E−02	2.36E−03	4.3687E−03	5.66E−04	4.4738E−03	2.19E−06
SDE	7.3459E−02	6.51E−03	5.5445E−02	5.94E−03	3.7505E−02	5.73E−03
ITLBO	1.4517E−02	2.10E−03	3.6661E−03	8.70E−04	4.4732E−03	1.66E−06
EJADE	1.5390E−03	1.88E−16	2.7465E−03	1.64E−16	4.4729E−03	2.31E−16
EGBO	1.5390E−03	**1.47E−16**	2.7465E−03	**1.52E−16**	4.4729E−03	**1.84E−16**

Table 14
Statistical results on case 2 at diverse irradiance and temperature of 25 °C.

Algorithm	200 W/m^2		400 W/m^2		600 W/m^2		800 W/m^2		1000 W/m^2	
	Mean	SD	Mean	SD	Mean	SD	Mean	SD	Mean	SD
JADE	1.0724E−03	1.28E−03	1.6400E−03	1.35E−03	1.8872E−03	2.33E−03	2.6748E−03	3.45E−03	6.6257E−03	7.32E−03
jDE	5.3852E−04	5.21E−05	2.3682E−03	1.95E−04	5.6230E−03	5.46E−04	6.6926E−03	8.13E−04	1.2654E−02	1.11E−03
SaDE	3.3074E−04	1.99E−05	1.1883E−03	2.21E−04	2.1748E−03	5.63E−04	2.5498E−03	6.25E−04	4.8556E−03	9.93E−04
AGDE	3.8306E−04	1.32E−04	1.3534E−03	5.01E−04	2.0227E−03	1.21E−03	2.8812E−03	1.40E−03	4.1891E−03	1.83E−03
SHADE	3.2069E−04	1.83E−09	7.6714E−04	5.21E−05	1.1130E−03	2.43E−04	1.2337E−03	2.80E−04	2.1635E−03	4.45E−04
SDE	2.3022E−03	7.41E−04	3.6726E−03	4.45E−04	8.5237E−03	6.93E−04	1.0485E−02	1.03E−03	2.0776E−02	3.06E−03
ITLBO	3.5639E−04	7.96E−05	1.2966E−03	3.83E−04	1.5947E−03	4.98E−04	2.2238E−03	1.07E−03	2.5960E−03	1.09E−03
EJADE	3.2069E−04	3.64E−18	7.0761E−04	5.70E−18	8.2395E−04	3.57E−17	6.6858E−04	5.36E−17	1.1462E−03	4.32E−17
EGBO	3.2069E−04	**3.05E−18**	7.0761E−04	8.88E−18	8.2395E−04	**3.93E−17**	6.6858E−04	**4.42E−17**	1.1462E−03	**3.16E−17**

Table 15
Statistical results on case 2 at dissimilar temperature and irradiance of 1000 W/m^2.

Algorithm	25 °C		50 °C		75 °C	
	Mean	SD	Mean	SD	Mean	SD
JADE	4.8187E−03	7.07E−03	5.5449E−03	3.31E−03	4.7044E−03	1.75E−03
jDE	1.2809E−02	1.40E−03	8.3895E−03	1.22E−03	5.4853E−03	6.28E−04
SaDE	4.7242E−03	1.30E−03	4.1941E−03	3.93E−04	3.7989E−03	5.27E−05
AGDE	5.6291E−03	2.97E−03	4.2406E−03	1.11E−03	3.7817E−03	5.93E−06
SHADE	2.0423E−03	4.14E−04	3.7903E−03	3.73E−06	3.7804E−03	6.02E−10
SDE	2.0415E−02	2.53E−03	1.5238E−02	2.08E−03	8.8431E−03	1.50E−03
ITLBO	2.2399E−03	1.08E−03	3.7990E−03	4.09E−05	3.7819E−03	8.02E−06
EJADE	1.1462E−03	4.07E−17	3.7888E−03	1.30E−16	3.7804E−03	1.24E−16
EGBO	1.1462E−03	**3.98E−17**	3.7888E−03	**7.92E−17**	3.7804E−03	**1.21E−16**

the MaxNFE equal to 30,000. EGBO has a faster convergence rate in the initial iterations than GBO for all models from this figure.

5.5. Results of experimental data extracted from the manufacturer's datasheet

Two distinct photovoltaic models (i.e., Multi-crystalline KC200GT (case 1) (Shell kc200gt, 2003) and Mono-crystalline SM55 (Shell, 2003) (case 2)) have been taken into account to examine that the developed EGBO performs promisingly and reliably. Extracting the *I-V* curves provides us with the experimental data of the two photovoltaic module models in the manufacturer's datasheet at diverse five irradiance and three temperature settings. The above standard optimizers are also used in this section as the comparing algorithms. Note that the MaxNFE is chosen to be equal to 30,000 in all of these optimizers as well. Other parameter values are the same as the original references. Additionally, the parameters' range is set as I_{ph} [0, 2*ISC*] (A), I_o [0, 100] (μA), R_s [0, 2] (Ω), R_{sh} [0, 5000] (Ω), and α [1, 4]. I_{SC} is the nonstandard conditions short circuit current related to irradiance (G) and temperature (T), which is attained in this way:

$$I_{SC}(G,T) = I_{SC\_STC} \times \frac{G}{G_{STC}} + a \times (T - T_{STC}) \tag{24}$$

where G_{STC} is irradiance, I_{SC_STC} denotes the short circuit current, T_{STC} refers to the temperature at standard test conditions, and a is the temperature coefficient of the short circuit current at the standard test conditions (Gupta et al., 2019).

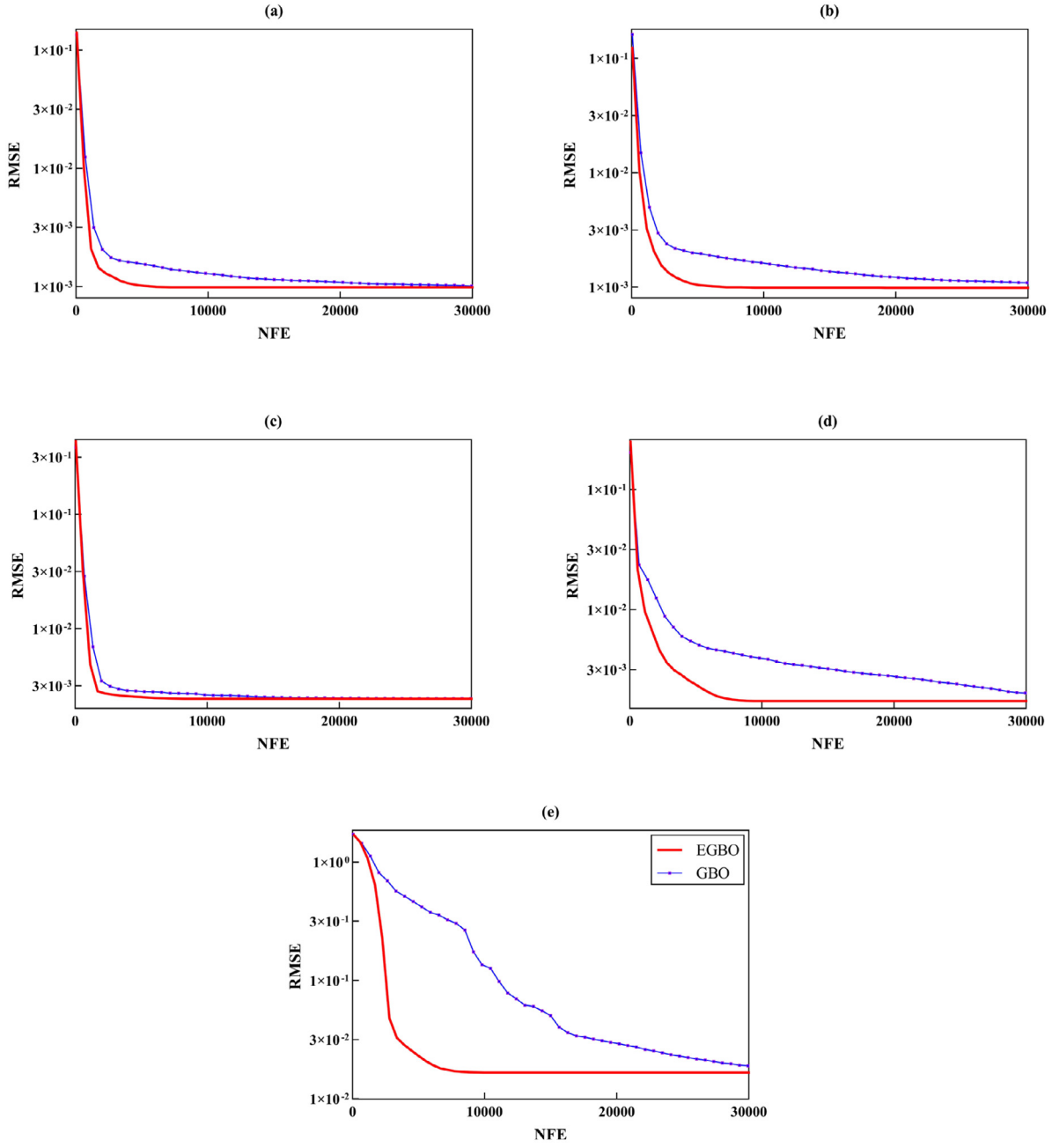

Fig. 10. Convergence curves for the EGBO and GBO algorithm for (a) M1, (b) M2, (c) M3, (d) M4, and (e) M5.

Tables 12–15 indicate the statistical results containing the mean and standard deviation of RMSE for all the methodologies. Based on these analyses, the developed EGBO gives promising and satisfactory results than other alternative algorithms available in the literature. A plus point is that Table 16 and Table 17 represent optimal extracted parameters using EJGBO at various irradiance and temperature, respectively. Fig. 11 and Fig. 12 respectively show the comparative analysis among simulated and measured data of 2 photovoltaic models at various irradiance and temperature.

Considering the results of Table 16, we can see that once irradiance increases, I_{ph} will be increased consequently while I_o, R_s, R_{sh}, and a, on the other hand, go up and down slightly. Additionally, it is evident that once temperature increases, then I_{ph} and Io will be enhanced accordingly when R_s, R_{sh}, and a are near-constant. Figs. 11 and 12 indicate that there is a remarkable coincidence between simulated and measured data. Admittedly, the developed EGBO algorithm provides precise parameter values while irradiance level is low, which is significant for the PV system's maximum power point tracking (MPPT). Some units in PV models are conditional on some mismatch circumstances, for example, partial shading. Furthermore, the derived and extracted results are utilized in the MPPT model for tuning and tracking the maximum power point, as temperature/radiation varying in actual applications. According to the exploratory properties of the proposed GBO, we can suggest other domains to apply to image-based and video-based processing (Yang et al., 2018; Jiang et al., 2018; Xu et al., 2018; Zuo et al., 2015, 2017). Also, more challenging domains with complex feature spaces such as video coding optimization (Zhou et al., 2019), remote sensing (Yang et al., 2019), image quality enhancement (Yang and Sowmya, 2015; Hu et al., 2020; Zhang et al., 2020g; Jiang et al., 2017), and dynamic

Table 16
Optimal parameters attained by the suggested EGBO for two PV units at diverse irradiance and temperature of 25 °C.

	Parameter	Mono-crystalline SM55	Multi-crystalline KC200GT
G = 200 W/m^2	I_{ph} (A)	6.91510E−01	1.64615E+00
	I_o (μA)	1.46412E−07	5.20997E−10
	R_s (Ω)	7.96166E−03	7.05762E−03
	R_{sh} (Ω)	1.24503E+01	1.27805E+01
	a	1.38066E+00	1.00324E+00
	RMSE	3.2069E−04	1.4185E−03
G = 400 W/m^2	I_{ph} (A)	1.38284E+00	3.28785E+00
	I_o (μA)	1.00420E−07	1.48987E−09
	R_s (Ω)	1.10182E−02	6.54775E−03
	R_{sh} (Ω)	1.18625E+01	1.39276E+01
	a	1.35199E+00	1.05504E+00
	RMSE	7.0761E−04	1.4262E−03
G = 600 W/m^2	I_{ph} (A)	2.07090E+00	4.93431E+00
	I_o (μA)	1.55514E−07	3.86144E−09
	R_s (Ω)	9.18063E−03	6.24700E−03
	R_{sh} (Ω)	1.25019E+01	1.37593E+01
	a	1.38753E+00	1.10402E+00
	RMSE	8.2395E−04	1.2977E−03
G = 800 W/m^2	I_{ph} (A)	2.76038E+00	6.57133E+00
	I_o (μA)	1.43951E−07	9.53063E−10
	R_s (Ω)	9.37751E−03	6.61732E−03
	R_{sh} (Ω)	1.27744E+01	1.37689E+01
	a	1.38114E+00	1.03532E+00
	RMSE	6.6858E−04	1.6310E−03
G = 1000 W/m^2	I_{ph} (A)	3.45010E+00	8.21689E+00
	I_o (μA)	1.71154E−07	2.24195E−09
	R_s (Ω)	9.14299E−03	6.36693E−03
	R_{sh} (Ω)	1.34417E+01	1.41395E+01
	a	1.39575E+00	1.07641E+00
	RMSE	1.1462E−03	1.5390E−03

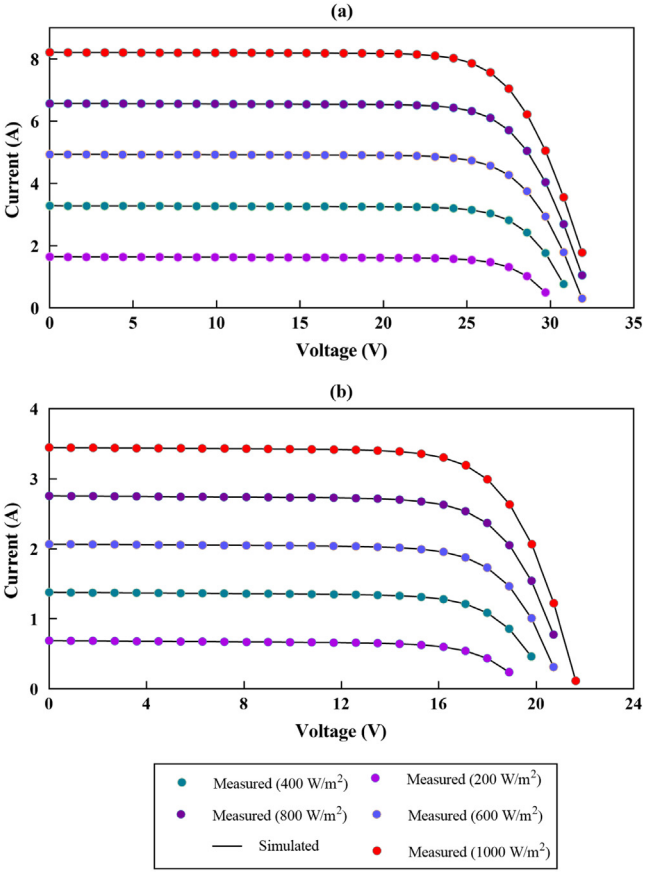

Fig. 11. Comparison between the I–V curves obtained by the EGBO versus measured data at various irradiance and temperature of 25 °C: (a) case 1, (b) case 2.

load identification (Wang et al., 2020a), phase imaging (Zhang et al., 2020h), control systems (Shi et al., 2017), and practical engineering problems (Zhang et al., 2020i; Zhao et al., 2020d) can be the next topics that the proposed GBO-based method can show its competency.

6. Conclusions and future directions

Extracting the parameters is among the critical tasks in the optimization of the photovoltaic systems. In this research, an enhanced gradient-based algorithm (EGBO) is first introduced to extract various PV models' uncertain parameters in a quick, precise, promising, and reliable way. In this algorithm, the rank-based mechanism is utilized to update the parameters efficiently, and the logistic, chaotic (LC) map is also adopted to improve the performance analysis of the former GBO algorithm. To validate the developed EGBO's promising performance, it has been employed successfully to extract the parameters of various photovoltaic models, such as the single diode model (SDM), the double diode model (DDM), and the PV module. The results indicate the superiority of the newly introduced EGBO over the original GBO algorithm, and it performs well compared to some other methods available in the literature. Testing on two photovoltaic module models at different irradiance and temperature has also shown it is another advantage, which is very beneficial and reliable in addressing the parameter extraction problem for different complicated photovoltaic cell models. Thus, the developed EGBO can be a reliable and promising alternative approach for parameter extraction of PV models. In general, the most significant insights into the results are listed as follows:

- Of all the optimizer algorithms, the proposed EGBO provides us with the best results, followed by the EJADE. The proposed method can then be a reliable alternative for other complicated parameter extraction problems of photovoltaic models.
- There exist two algorithmic parameters in the EGBO (i.e., F_1 and F_2). For updating these parameters at each iteration, an efficient mechanism has been introduced in this research, resulting in better performance analysis than the original GBO algorithm. Motivated by this phenomenon, we can develop a more sophisticated adaptive mechanism for enhancing the performance analysis of GBO for complicated problems in PV systems.
- For implementing the MELO randomly, the EGBO utilized the LC map. Various published works claimed that the chaotic maps could easily escape from the local minima (Zhao et al., 2020a; Abdollahi and Ahmadianfar, 2021). Hence, the implementation of this LC map can help the proposed EGBO to explore the promising regions in the solution space.
- Regarding the computational and processing time, ITLBO, jDE, and AGDE are faster than algorithms for all models. Moreover, although EGBO is not the fastest algorithm, it can obtain the best results.

Additionally, under the PV system's partial shading, the challenging condition is not considered in this research. Consequently, in future research, the proposed EGBO will perform a practical experiment to tackle more complex PV problems with these properties and other energy optimization cases (Ram et al., 2017), particularly for the maximum power point tracking (MPPT) problem in the PV models. We will also use oppositional learning to more enhance the EGBO performance. Besides, dynamic population size can be employed in the EGBO to improve its efficiency in solving complex problems.

Table 17
Best parameters attained by proposed EGBO method for two PV models at dissimilar temperature and irradiance of 1000 W/m^2.

PV module	Temperature	I_{ph} (A)	I_o (μA)	R_s (Ω)	R_{sh} (Ω)	a	RMSE
Mono-crystalline SM55	25 °C	3.450104	1.71154E−07	0.009143	13.441679	1.395753	1.1462E−03
	40 °C	3.469138	1.14511E−06	0.008697	14.807478	1.417840	3.7888E−03
	60 °C	3.494608	6.90950E−06	0.008853	13.469000	1.405142	3.7804E−03
Multi-crystalline KC200GT	25 °C	8.216891	2.24195E−09	0.006367	14.139540	1.07641	1.5390E−03
	50 °C	8.295305	1.25953E−07	0.006216	17.664627	1.117292	2.7465E−03
	75 °C	8.377663	1.63082E−06	0.006343	14.639969	1.10148	4.4729E−03

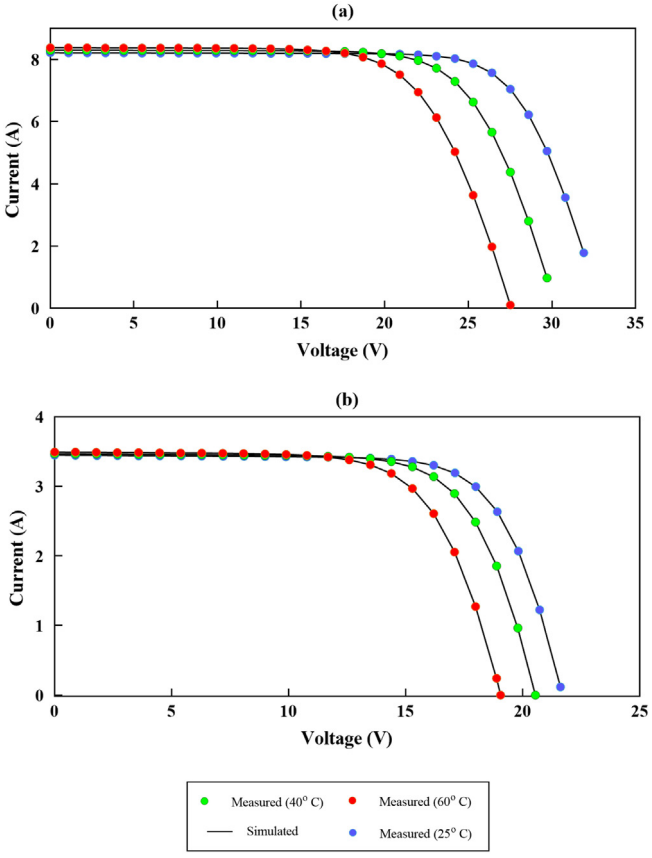

Fig. 12. Comparison between the I–V curves obtained by the EGBO versus measured data at various temperatures and irradiance of 1000 W/m^2: (a) case 1, (b) case 2.

CRediT authorship contribution statement

Iman Ahmadianfar: Conceptualization, Methodology, Validation, Writing - original draft, Writing - review & editing, Software, Investigation. **Wenyin Gong:** Writing - original draft, Writing - review & editing, Software. **Ali Asghar Heidari:** Project administration, Conceptualization, Validation, Supervision, Methodology, Formal analysis, Resources, Data Curation, Writing - original draft, Writing - review & editing, Software, Visualization, Investigation. **Noorbakhsh Amiri Golilarz:** Writing - original draft, Writing - review & editing, Investigation. **Arvin Samadi-Koucheksaraee:** Validation, Writing - original draft, Writing - review & editing. **Huiling Chen:** Validation, Conceptualization, Methodology, Formal analysis, Investigation, Writing - review & editing, Funding acquisition, Supervision.

Declaration of competing interest

The authors declare that they have no known competing financial interests or personal relationships that could have appeared to influence the work reported in this paper.

References

Abbassi, R., et al., 2019. An efficient salp swarm-inspired algorithm for parameters identification of photovoltaic cell models. Energy Convers. Manage. 179, 362–372.
Abbassi, A., et al., 2020. Parameters identification of photovoltaic cell models using enhanced exploratory salp chains-based approach. Energy 117333.
Abdollahi, A., Ahmadianfar, I., 2021. Multi-mechanism ensemble interior search algorithm to derive optimal hedging rule curves in multi-reservoir systems. J. Hydrol. 126211.
Ahmadianfar, I., Bozorg-Haddad, O., Chu, X., 2019b. Optimizing multiple linear rules for Multi-Reservoir hydropower systems using an optimization method with an adaptation strategy. Water Resour. Manage. 33 (12), 4265–4286.
Ahmadianfar, I., Bozorg-Haddad, O., Chu, X., 2020a. Gradient-based optimizer: A new metaheuristic optimization algorithm. Inform. Sci. 540, 131–159.
Ahmadianfar, I., et al., 2019a. Developing optimal policies for reservoir systems using a multi-strategy optimization algorithm. Appl. Soft Comput. 80, 888–903.
Ahmadianfar, I., et al., 2020b. Optimizing operating rules for multi-reservoir hydropower generation systems: An adaptive hybrid differential evolution algorithm. Renew. Energy.
Ahmadianfar, I., et al., 2021. RUN beyond the metaphor: An efficient optimization algorithm based on Runge Kutta method. Expert Syst. Appl. 115079.
Aljarah, I., Mafarja, M., Heidari, A.A., Faris, H., Mirjalili, S., 2020. Multi-verse optimizer: theory, literature review, and application in data clustering. Nature-inspired Optim. 123–141.
Ba, A.F., et al., 2020. Levy-based antlion-inspired optimizers with orthogonal learning scheme. Eng. Comput. 1–22.
Campana, P.E., et al., 2019. Optimization and assessment of floating and floating-tracking PV systems integrated in on-and off-grid hybrid energy systems. Sol. Energy 177, 782–795.
Chen, H., Jiao, S., Heidari, A.A., Wang, M., Chen, X., Zhao, X., 2019b. An opposition-based sine cosine approach with local search for parameter estimation of photovoltaic models. Energy Convers. Manage. 195, 927–942.
Chen, H., Jiao, S., Wang, M., Heidari, A.A., Zhao, X., 2020. Parameters identification of photovoltaic cells and modules using diversification-enriched harris hawks optimization with chaotic drifts. J. Clean. Prod. 244, 118778.
Chen, X., Yu, K., 2019. Hybridizing cuckoo search algorithm with biogeography-based optimization for estimating photovoltaic model parameters. Sol. Energy 180, 192–206.
Chen, X., et al., 2016. Parameters identification of solar cell models using generalized oppositional teaching learning based optimization. Energy 99, 170–180.
Chen, X., et al., 2018. Teaching–learning–based artificial bee colony for solar photovoltaic parameter estimation. Appl. Energy 212, 1578–1588.
Chen, M., et al., 2019a. A two-layer nonlinear combination method for short-term wind speed prediction based on ELM, ENN, and LSTM. IEEE Internet Things J. 6 (4), 6997–7010.
Chen, H., et al., 2020a. Multi-population differential evolution-assisted Harris hawks optimization: Framework and case studies. Future Gener. Comput. Syst. 111, 175–198.
Chen, H., et al., 2020b. Parameters identification of photovoltaic cells and modules using diversification-enriched harris hawks optimization with chaotic drifts. J. Cleaner Prod. 244.
Chen, Y., et al., 2021. Large group activity security risk assessment and risk early warning based on random forest algorithm. Pattern Recognit. Lett. 144, 1–5.

Chin, V.J., Salam, Z., Ishaque, K., 2015. Cell modelling and model parameters estimation techniques for photovoltaic simulator application: A review. Appl. Energy 154, 500–519.

Deng, R., Li, M., Linghu, S., 2021. Sensitivity analysis of steam injection parameters of steam injection thermal recovery technology. Fresenius Environ. Bull. 30 (05), 5385–5394.

Deng, W., et al., 2020a. A novel gate resource allocation method using improved PSO-based QEA. IEEE Trans. Intell. Transp. Syst. http://dx.doi.org/10.1109/TITS.2020.3025796.

Deng, W., et al., 2020b. An improved quantum-inspired differential evolution algorithm for deep belief network. IEEE Trans. Instrum. Meas. http://dx.doi.org/10.1109/TIM.2020.2983233.

Dkhichi, F., et al., 2014. Parameter identification of solar cell model using Levenberg–Marquardt algorithm combined with simulated annealing. Sol. Energy 110, 781–788.

Easwarakhanthan, T., et al., 1986. Nonlinear minimization algorithm for determining the solar cell parameters with microcomputers. Int. J. Sol. Energy 4 (1), 1–12.

El-Naggar, K.M., et al., 2012. Simulated annealing algorithm for photovoltaic parameters identification. Sol. Energy 86 (1), 266–274.

Fan, Y., Wang, P., Heidari, A.A., Zhao, X., Turabieh, H., Chen, H., 2021. Delayed dynamic step shuffling frog-leaping algorithm for optimal design of photovoltaic models. Energy Rep. 7, 228–246.

Gao, X., et al., 2018. Parameter extraction of solar cell models using improved shuffled complex evolution algorithm. Energy Convers. Manage. 157, 460–479.

Gupta, S., et al., 2019. Harmonized salp chain-built optimization. Eng. Comput. 1–31.

Heidari, A.A., Abbaspour, R.A., Chen, H., 2019b. Efficient boosted grey wolf optimizers for global search and kernel extreme learning machine training. Appl. Soft Comput. 81, 105521.

Heidari, A.A., et al., 2019a. Harris hawks optimization: Algorithm and applications. Future Gener. Comput. Syst. 97, 849–872.

Hestenes, M.R., Stiefel, E., 1952. Methods of Conjugate Gradients for Solving Linear Systems, Vol. 49. NBS Washington, DC.

Hu, L., et al., 2017. A new machine-learning method to prognosticate paraquat poisoned patients by combining coagulation, liver, and kidney indices. Plos One 12 (10), e0186427.

Hu, X., et al., 2019. An integrated step-up inverter without transformer and leakage current for grid-connected photovoltaic system. IEEE Trans. Power Electron. 34 (10), 9814–9827.

Hu, Y., et al., 2020. Microscopic fringe projection profilometry: A review. Opt. Lasers Eng. 106192.

Hu, J., et al., 2021. Orthogonal learning covariance matrix for defects of grey wolf optimizer: insights, balance, diversity, and feature selection. Knowl.-Based Syst. 213, 106684.

Huang, Z., et al., 2021. Parameter analysis of damaged region for laminates with matrix defects. J. Sandwich Struct. Mater. 23 (2), 580–620.

Humada, A.M., et al., 2016. Solar cell parameters extraction based on single and double-diode models: A review. Renew. Sustain. Energy Rev. 56, 494–509.

Jiang, P., Chen, J., 2016. Displacement prediction of landslide based on generalized regression neural networks with K-fold cross-validation. Neurocomputing 198, 40–47.

Jiang, L.L., Maskell, D.L., Patra, J.C., 2013. Parameter estimation of solar cells and modules using an improved adaptive differential evolution algorithm. Appl. Energy 112, 185–193.

Jiang, Q., et al., 2017. Optimizing multistage discriminative dictionaries for blind image quality assessment. IEEE Trans. Multimed. 20 (8), 2035–2048.

Jiang, Q., et al., 2018. Unified no-reference quality assessment of singly and multiply distorted stereoscopic images. IEEE Trans. Image Process. 28 (4), 1866–1881.

Jiao, S., et al., 2020. Orthogonally adapted Harris hawks optimization for parameter estimation of photovoltaic models. Energy 203, 117804.

Jordehi, A.R., Jasni, J., 2012. Approaches for FACTS optimization problem in power systems. In: 2012 IEEE International Power Engineering and Optimization Conference Melaka, Malaysia. IEEE, pp. 355–360.

Kordestani, H., Zhang, C., 2020. Direct use of the Savitzky–Golay filter to develop an output-only trend line-based damage detection method. Sensors 20 (7), 1983.

Li, S., Gong, W., Wang, L., Yan, X., Hu, C., 2020. A hybrid adaptive teaching–learning-based optimization and differential evolution for parameter identification of photovoltaic models. Energy Convers. Manage. 225, 113474.

Li, Q., et al., 2017. An enhanced grey wolf optimization based feature selection wrapped kernel extreme learning machine for medical diagnosis. Comput. Math. Methods Med. 2017.

Li, C., et al., 2018. Developing a new intelligent system for the diagnosis of tuberculous pleural effusion. Comput. Methods Programs Biomed. 153, 211–225.

Li, S., et al., 2019a. Parameter extraction of photovoltaic models using an improved teaching-learning-based optimization. Energy Convers. Manage. 186, 293–305.

Li, T., et al., 2019b. A deep learning approach for multi-frame in-loop filter of HEVC. IEEE Trans. Image Process. 28 (11), 5663–5678.

Li, S., et al., 2020a. Slime mould algorithm: A new method for stochastic optimization. Future Gener. Comput. Syst. 111, 300–323.

Li, S., et al., 2020b. An enhanced adaptive differential evolution algorithm for parameter extraction of photovoltaic models. Energy Convers. Manage. 205, 112443.

Liang, X., et al., 2020. Chaotic oppositional sine–cosine method for solving global optimization problems. Eng. Comput. 1–17.

Lin, A., et al., 2019. Predicting intentions of students for master programs using a chaos-induced sine cosine-based fuzzy K-nearest neighbor classifier. Ieee Access 7, 67235–67248.

Liu, Y., Chong, G., Heidari, A.A., Chen, H., Liang, G., Ye, X., Wang, M., 2020. Horizontal and vertical crossover of Harris hawk optimizer with Nelder-Mead simplex for parameter estimation of photovoltaic models. Energy Convers. Manage. 223, 113211.

Liu, Y., Heidari, A.A., Ye, X., Liang, G., Chen, H., He, C., 2021. Boosting Slime Mould Algorithm for Parameter Identification of Photovoltaic Models. Energy 121164.

Ma, X., et al., 2021. Data-driven niching differential evolution with adaptive parameters control for history matching and uncertainty quantification. SPE J. 26 (02), 993–1010.

Mafarja, M., Heidari, A.A., Faris, H., Mirjalili, S., Aljarah, I., 2020. Dragonfly algorithm: theory, literature review, and application in feature selection. Nature-inspired Optim. 47–67.

Mohamed, A.W., Mohamed, A.K., 2019. Adaptive guided differential evolution algorithm with novel mutation for numerical optimization. Int. J. Mach. Learn. Cybern. 10 (2), 253–277.

Muhsen, D.H., et al., 2016. A comparative study of evolutionary algorithms and adapting control parameters for estimating the parameters of a single-diode photovoltaic module's model. Renew. Energy 96, 377–389.

Nama, S., Saha, A.K., Ghosh, S., 2017. Improved backtracking search algorithm for pseudo dynamic active earth pressure on retaining wall supporting c-ϕ. Appl. Soft Comput. 52, 885–897.

Nautiyal, B., et al., 2021. Improved Salp Swarm Algorithm with mutation schemes for solving global optimization and engineering problems. Eng. Comput. 1–23.

Niu, Q., Zhang, H., Li, K., 2014. An improved TLBO with elite strategy for parameters identification of PEM fuel cell and solar cell models. Int. J. Hydrogen Energy 39 (8), 3837–3854.

Oliva, D., Cuevas, E., Pajares, G., 2014. Parameter identification of solar cells using artificial bee colony optimization. Energy 72, 93–102.

Omran, M.G., Salman, A., Engelbrecht, A.P., 2005. Self-adaptive differential evolution. In: International Conference on Computational and Information Science. Springer.

Özban, A.Y., 2004. Some new variants of Newton's method. Appl. Math. Lett. 17 (6), 677–682.

Pang, J., et al., 2018. A scatter simulated annealing algorithm for the bi-objective scheduling problem for the wet station of semiconductor manufacturing. Comput. Ind. Eng. 123, 54–66.

Qais, M.H., Hasanien, H.M., Alghuwainem, S., 2019b. Identification of electrical parameters for three-diode photovoltaic model using analytical and sunflower optimization algorithm. Appl. Energy 250, 109–117.

Qais, M.H., Hasanien, H.M., Alghuwainem, S., 2020a. Parameters extraction of three-diode photovoltaic model using computation and Harris hawks optimization. Energy 195, 117040.

Qais, M.H., Hasanien, H.M., Alghuwainem, S., 2020b. Transient search optimization for electrical parameters estimation of photovoltaic module based on datasheet values. Energy Convers. Manage. 214, 112904.

Qais, M.H., et al., 2019a. Coyote optimization algorithm for parameters extraction of three-diode photovoltaic models of photovoltaic modules. Energy 187, 116001.

Qin, A.K., Suganthan, P.N., 2005. Self-adaptive differential evolution algorithm for numerical optimization. In: 2005 IEEE Congress on Evolutionary Computation. IEEE.

Qu, S., et al., 2021. Design and implementation of a fast sliding-mode speed controller with disturbance compensation for SPMSM system. IEEE Trans. Transp. Electr.

Rajasekar, N., Kumar, N.K., Venugopalan, R., 2013. Bacterial foraging algorithm based solar PV parameter estimation. Sol. Energy 97, 255–265.

Ram, J.P., Babu, T.S., Rajasekar, N., 2017. A comprehensive review on solar PV maximum power point tracking techniques. Renew. Sustain. Energy Rev. 67, 826–847.
Ridha, H.M., Gomes, C., Hizam, H., Ahmadipour, M., Heidari, A.A., Chen, H., 2021a. Multi-objective optimization and multi-criteria decision-making methods for optimal design of standalone photovoltaic system: A comprehensive review. Renew. Sustain. Energy Rev. 135, 110202.
Ridha, H.M., Hizam, H., Gomes, C., Heidari, A.A., Chen, H., Ahmadipour, M., Alghrairi, M., 2021b. Parameters extraction of three diode photovoltaic models using boosted LSHADE algorithm and Newton Raphson method. Energy 224, 120136.
Ridha, H.M., et al., 2020. Boosted mutation-based Harris hawks optimizer for parameters identification of single-diode solar cell models. Energy Convers. Manage. 209, 112660.
Rodriguez-Esparza, E., et al., 2020. An efficient Harris hawks-inspired image segmentation method. Expert Syst. Appl. 155, 113428.
Selem, S.I., El-Fergany, A.A., Hasanien, H.M., 2021. Artificial electric field algorithm to extract nine parameters of triple-diode photovoltaic model. Int. J. Energy Res. 45 (1), 590–604.
Shan, W., Qiao, Z., Heidari, A.A., Chen, H., Turabieh, H., Teng, Y., 2021. Double adaptive weights for stabilization of moth flame optimizer: balance analysis, engineering cases, and medical diagnosis. Knowl.-Based Syst. 214, 106728.
Shell kc200gt photovoltaic solar module, 2003. (Accessed June 2021).
Shell sm55 photovoltaic solar module, 2003. URL https://aeet-service.com/pdf/shell/Shell-Solar_SM55.pdf.
Shi, K., et al., 2017. Secondary delay-partition approach on robust performance analysis for uncertain time-varying Lurie nonlinear control system. Optim. Control Appl. Methods 38 (6), 1208–1226.
Song, S., et al., 2020. Dimension decided Harris hawks optimization with Gaussian mutation: Balance analysis and diversity patterns. Knowl.-Based Syst. 106425. http://dx.doi.org/10.1016/j.knosys.2020.106425.
Tanabe, R., Fukunaga, A., 2013. Success-history based parameter adaptation for differential evolution. In: 2013 IEEE Congress on Evolutionary Computation. IEEE.
Tang, L., Dong, Y., Liu, J., 2014. Differential evolution with an individual-dependent mechanism. IEEE Trans. Evol. Comput. 19 (4), 560–574.
Tong, N.T., Pora, W., 2016. A parameter extraction technique exploiting intrinsic properties of solar cells. Appl. Energy 176, 104–115.
Tu, J., Chen, H., Liu, J., Heidari, A.A., Zhang, X., Wang, M., Pham, Q.V., 2021. Evolutionary biogeography-based whale optimization methods with communication structure: towards measuring the balance. Knowl.-Based Syst. 212, 106642.
Tu, J., et al., 2019. Predict the entrepreneurial intention of fresh graduate students based on an adaptive support vector machine framework. Math. Probl. Eng. 2019, 1–16.
Wang, M., Zhao, X., Heidari, A.A., Chen, H., 2020b. Evaluation of constraint in photovoltaic models by exploiting an enhanced ant lion optimizer. Sol. Energy 211, 503–521.
Wang, M., et al., 2017a. Grey wolf optimization evolving kernel extreme learning machine: Application to bankruptcy prediction. Eng. Appl. Artif. Intell. 63, 54–68.
Wang, M., et al., 2017b. Toward an optimal kernel extreme learning machine using a chaotic moth-flame optimization strategy with applications in medical diagnoses. Neurocomputing 267, 69–84.
Wang, L., et al., 2020a. A new regularization method for dynamic load identification. Sci. Progress 103 (3), 0036850420931283.
Wei, H., et al., 2011. Extracting solar cell model parameters based on chaos particle swarm algorithm. In: 2011 International Conference on Electric Information and Control Engineering. IEEE.
Wei, Y., et al., 2017. An improved grey wolf optimization strategy enhanced SVM and its application in predicting the second major. Math. Probl. Eng. 2017, 1–12.
Wei, Y., et al., 2020. Predicting entrepreneurial intention of students: An extreme learning machine with Gaussian barebone Harris hawks optimizer. IEEE Access 8, 76841–76855.
Weng, X., Heidari, A.A., Liang, G., Chen, H., Ma, X., Mafarja, M., Turabieh, H., 2021. Laplacian Nelder-Mead spherical evolution for parameter estimation of photovoltaic models. Energy Convers. Manage. 243, 114223.
Xu, S., Wang, Y., 2017. Parameter estimation of photovoltaic modules using a hybrid flower pollination algorithm. Energy Convers. Manage. 144, 53–68.
Xu, M., et al., 2018. Assessing visual quality of omnidirectional videos. IEEE Trans. Circuits Syst. Video Technol. 29 (12), 3516–3530.
Xu, Y., et al., 2019. An efficient chaotic mutative moth-flame-inspired optimizer for global optimization tasks. Expert Syst. Appl. 129, 135–155.
Xue, X., et al., 2020. Affine transformation-enhanced multifactorial optimization for heterogeneous problems. IEEE Trans. Cybern..
Yang, M., Sowmya, A., 2015. An underwater color image quality evaluation metric. IEEE Trans. Image Process. 24 (12), 6062–6071.
Yang, R., et al., 2018. Enhancing quality for HEVC compressed videos. IEEE Trans. Circuits Syst. Video Technol. 29 (7), 2039–2054.
Yang, Y., et al., 2019. Omnidirectional motion classification with monostatic radar system using micro-Doppler signatures. IEEE Trans. Geosci. Remote Sens. 58 (5), 3574–3587.
Yang, Y., et al., 2021. Hunger games search: Visions, conception, implementation, deep analysis, perspectives, and towards performance shifts. Expert Syst. Appl. 177, 114864.
Yu, K., et al., 2017a. Parameters identification of photovoltaic models using self-adaptive teaching-learning-based optimization. Energy Convers. Manage. 145, 233–246.
Yu, K., et al., 2017b. Parameters identification of photovoltaic models using an improved JAYA optimization algorithm. Energy Convers. Manage. 150, 742–753.
Yu, K., et al., 2018. Multiple learning backtracking search algorithm for estimating parameters of photovoltaic models. Appl. Energy 226, 408–422.
Yu, C., et al., 2021a. Boosting quantum rotation gate embedded slime mould algorithm. Expert Syst. Appl. 115082.
Yu, C., et al., 2021b. SGOA: annealing-behaved grasshopper optimizer for global tasks. Eng. Comput. http://dx.doi.org/10.1007/s00366-020-01234-1.
Zeng, G.-q., Lu, Y.-z., Mao, W.-J, 2011. Modified extremal optimization for the hard maximum satisfiability problem. J. Zhejiang Univ. Sci. C 12 (7), 589–596.
Zeng, G., et al., 2012. Backbone guided extremal optimization for the hard maximum satisfiability problem. Int. J. Innovative Comput. Inf. Control 8 (12), 8355–8366.
Zeng, G.-Q., et al., 2014. Binary-coded extremal optimization for the design of PID controllers. Neurocomputing 138, 180–188.
Zeng, G.-Q., et al., 2015. Design of fractional order PID controller for automatic regulator voltage system based on multi-objective extremal optimization. Neurocomputing 160, 173–184.
Zeng, G.-Q., et al., 2019. Adaptive population extremal optimization-based PID neural network for multivariable nonlinear control systems. Swarm Evol. Comput. 44, 320–334.
Zhang, H., Heidari, A.A., Wang, M., Zhang, L., Chen, H., Li, C., 2020k. Orthogonal Nelder-Mead moth flame method for parameters identification of photovoltaic modules. Energy Convers. Manage. 211, 112764.
Zhang, Z., Luo, C., Zhao, Z., 2020a. Application of probabilistic method in maximum tsunami height prediction considering stochastic seabed topography. Nat. Hazards 104 (3), 2511–2530.
Zhang, Z., et al., 2020b. Dynamic reliability analysis of nonlinear structures using a Duffing-system-based equivalent nonlinear system method. Internat. J. Approx. Reason. 126, 84–97.
Zhang, Y., et al., 2020c. Boosted binary Harris hawks optimizer and feature selection. Eng. Comput. 1–30.
Zhang, X., et al., 2020d. Gaussian mutational chaotic fruit fly-built optimization and feature selection. Expert Syst. Appl. 141, 112976.
Zhang, H., et al., 2020e. A multi-strategy enhanced salp swarm algorithm for global optimization. Eng. Comput. 1–27.
Zhang, H., et al., 2020f. Orthogonal Nelder–Mead moth flame method for parameters identification of photovoltaic modules. Energy Convers. Manage. 211.
Zhang, J., et al., 2020g. Resolution analysis in a lens-free on-chip digital holographic microscope. IEEE Trans. Comput. Imaging 6, 697–710.
Zhang, J., et al., 2020h. On a universal solution to the transport-of-intensity equation. Opt. Lett. 45 (13), 3649–3652.
Zhang, Z., et al., 2020i. Time interval of multiple crossings of the Wiener process and a fixed threshold in engineering. Mech. Syst. Signal Process. 135, 106389.
Zhang, Y., et al., 2020j. Towards augmented kernel extreme learning models for bankruptcy prediction: algorithmic behavior and comprehensive analysis. Neurocomputing http://dx.doi.org/10.1016/j.neucom.2020.10.038.
Zhang, Y., et al., 2021a. Towards augmented kernel extreme learning models for bankruptcy prediction: algorithmic behavior and comprehensive analysis. Neurocomputing 430, 185–212.
Zhang, K., et al., 2021b. History matching of naturally fractured reservoirs using a deep sparse autoencoder. SPE J. 1–22.
Zhao, W., Wang, L., Zhang, Z., 2019a. A novel atom search optimization for dispersion coefficient estimation in groundwater. Future Gener. Comput. Syst. 91, 601–610.
Zhao, X., et al., 2019b. Chaos enhanced grey wolf optimization wrapped ELM for diagnosis of paraquat-poisoned patients. Comput. Biol. Chem. 78, 481–490.
Zhao, H., et al., 2019c. Performance prediction using high-order differential mathematical morphology gradient spectrum entropy and extreme learning machine. IEEE Trans. Instrum. Meas. http://dx.doi.org/10.1109/TIM.2019.2948414.

Zhao, D., et al., 2020a. Chaotic random spare ant colony optimization for multi-threshold image segmentation of 2D kapur entropy. Knowl.-Based Syst. 106510. http://dx.doi.org/10.1016/j.knosys.2020.106510.

Zhao, D., et al., 2020b. Ant colony optimization with horizontal and vertical crossover search: Fundamental visions for multi-threshold image segmentation. Expert Syst. Appl. 114122.

Zhao, D., et al., 2020c. Ant colony optimization with horizontal and vertical crossover search: Fundamental visions for multi-threshold image segmentation. Expert Syst. Appl. 114122. http://dx.doi.org/10.1016/j.eswa.2020.114122.

Zhao, J., et al., 2020d. Efficient deployment with geometric analysis for mmWave UAV communications. IEEE Wirel. Commun. Lett. 9 (7), 1115–1119.

Zhao, S., et al., 2021. Multilevel threshold image segmentation with diffusion association slime mould algorithm and Renyi's entropy for chronic obstructive pulmonary disease. Comput. Biol. Med. 104427.

Zhou, H., et al., 2018. A modified particle swarm optimization algorithm for a batch-processing machine scheduling problem with arbitrary release times and non-identical job sizes. Comput. Ind. Eng. 123, 67–81.

Zhou, Y., et al., 2019. Video coding optimization for virtual reality 360-degree source. IEEE J. Sel. Top. Sign. Proces. 14 (1), 118–129.

Zhou, W., et al., 2021. Random learning gradient based optimization for efficient design of photovoltaic models. Energy Convers. Manage. 230, 113751.

Zhu, W., et al., 2020. Evaluation of sino foreign cooperative education project using orthogonal sine cosine optimized kernel extreme learning machine. IEEE Access 8, 61107–61123.

Zou, F., et al., 2015. Teaching–learning-based optimization with learning experience of other learners and its application. Appl. Soft Comput. 37, 725–736.

Zuo, C., et al., 2015. Transport of intensity phase retrieval and computational imaging for partially coherent fields: The phase space perspective. Opt. Lasers Eng. 71, 20–32.

Zuo, C., et al., 2017. High-resolution transport-of-intensity quantitative phase microscopy with annular illumination. Sci. Rep. 7 (1), 1–22.